MECHANISTIC STUDY OF RND3 IN CARDIOMYOPATHY

A Dissertation

by

XIAOJING YUE

Submitted to the Office of Graduate and Professional Studies of
Texas A&M University
in partial fulfillment of the requirements for the degree of

DOCTOR OF PHILOSOPHY

Chair of Committee,	Jiang Chang
Committee Members,	Xia Lin
	Jianming Xu
	Dekai Zhang
Head of Department,	Van Wilson

May 2015

Major Subject: Medical Sciences

ABSTRACT

In human end-stage heart failure patients, the activation of Rho kinase 1 (ROCK1) is observed in the heart. ROCK1 activation promotes the activation of caspase 3, which results in a feed-forward loop contributing to myocyte apoptosis. Rnd3, a small GTPase, is an endogenous inhibitor of ROCK1. I observed a decrease in Rnd3 protein levels in human failing hearts, suggesting a pathological significance of Rnd3 alteration in the transition to heart failure. However, the biological function of Rnd3 in the heart remains unexplored. To investigate the functional role of Rnd3 in the heart and the underlying mechanism, the Rnd3 knockout mouse line was generated to mimic the down-regulation of Rnd3 in the diseased human heart. Rnd3 deficiency ($Rnd3^{-/-}$) resulted in embryonic lethality. Severe cardiac apoptosis along with elevated ROCK1 activity were observed in the $Rnd3^{-/-}$ mice at the E10.5 stage. The haploinsufficient ($Rnd3^{+/-}$) mice were viable, however, were predisposed to heart failure after transverse aortic constriction (TAC) induced hemodynamic stress. Remarkable cardiomyocyte apoptosis, increased caspase 3 activity, and activation of ROCK1 were detected in the $Rnd3^{+/-}$ heart compared to the wild-type (WT) control. Pharmacological inhibition of ROCK1 by Fasudil administration partially improved cardiac function and attenuated apoptosis in the $Rnd3^{+/-}$ mice after TAC. To determine whether ROCK1 contributed to the Rnd3 deficiency-mediated heart failure and cardiac apoptosis, I generated a double knockout (DKO) mouse line with $Rnd3^{+/-\ ROCK1-/-}$ background. Again, the genetic deletion of *ROCK1* partially rescued the phenotype. My data suggest that Rnd3 is a novel anti-

apoptotic factor that protects the heart from cardiac apoptosis partially through the inhibition of the ROCK1 pathway.

Determining the ROCK1 independent mechanisms involved in the Rnd3 deficiency-mediated cardiac remodeling is the goal for further investigation. Compensatory angiogenesis is necessary in the cardiac response to the ischemic stimuli. Compared to the wild-type mice, the post-TAC Rnd3$^{+/-}$ hearts showed significantly smaller capillary areas, fewer capillary numbers, a 20.8% reduction of coronary flow reserve, and a 5.9-fold increase in the hypoxic myocardial areas. Key pro-angiogenic factors were down-regulated, including hypoxia-inducible factor 1α (HIF1α) and vascular endothelial growth factor A (VEGFA), suggesting a stress-responsive angiogenic defect. Using loss- and gain-of-function approaches, I revealed that Rnd3 physically interacted with and stabilized HIF1α. The deficiency of Rnd3 facilitated the HIF1α protein degradation, reduced the VEGFA expression, and compromised the endothelial cell tube formation. Finally, the angiogenesis defect and the heart failure phenotype in the Rnd3$^{+/-}$ mice were partially rescued by cobalt chloride treatment, a HIF1α stabilizer. My data suggests that Rnd3 is a pro-angiogenic factor involved in the responsive angiogenesis in the heart through HIF1α-VEGF signaling promotion. Animals with Rnd3 haploinsufficiency showed cardiac dysfunction with impaired angiogenesis in response to the pressure overload. The down-regulation of Rnd3 observed in the heart failure patients may explain the insufficiency in the compensatory angiogenesis, which contributes to the transition to heart failure.

DEDICATION

I dedicate this dissertation to my family, my mentor, and all of my friends.

Especially to my father and mother for instilling the importance of hard work and higher education;

To my grandfather and grandmother for the encouragement;

To Dr. Jiang Chang for his guidance and care;

To Xiangsheng Yang and Xi Lin for their friendship and kind help;

To Guangyu, may you achieve your dreams.

ACKNOWLEDGEMENTS

This work has been carried out at the Texas A&M University Health Science Center Institute of Bioscience and Technology under the guidance of Dr. Jiang Chang during the years 2010-2015. Support for this research was provided by Grants: the American Heart Association Grant-in-Aid 0855030F, the NIH-NHLBI R01HL102314, the NIH-NHLBI R01HL123953, and the NIH-K02HL098956 to Jiang Chang; the American Heart Association Postdoctoral Fellowship 13POST17260043 to Xiangsheng Yang; the China Scholarship Council Fellowship to Xiaojing Yue; the National Natural Science Foundation of China 81460070 to Tianfa Li, 1160020 and 81460042 to Junli Guo.

First of all, I would like to express my sincere gratitude from the deepest part of my heart to my mentor, Dr. Jiang Chang, for offering me a precious opportunity to join his group; for his mentoring during the this five-year study; for his encouragement whenever there were rainy days; for his inspiration whenever there was confusion. Dr. Chang is more than just a mentor in the lab. He encouraged me while attending scientific conferences to explore the most advanced research progressions. He is also a great supervisor that guided me in public presentation, research paper writing, and early career development. I am so lucky to have him as my graduate advisor. Secondly, let me express my sincere thanks to my graduate advisor committee members. Dr. Jianming Xu inspires me with his millions of questions. Dr. Dekai Zhang encourages me. Dr. Xia Lin treats me as her own child. I still remember her gentle words of comfort when I sprained

my ankle a few months ago. Without their time, comments, and support, I could never make it today. Thirdly, all members in Dr. Chang's group, their friendship and kindness really mean a lot to me. Dr. Xiangsheng Yang, also my fiancé, encouraged me to overcome my shyness and to become an independent strong woman. Dr. Xi Lin, one of my best friends, always helped us to move our work forward and took care of us in our life. Kelsey Andrade, our manager, provided me suggestions for my paper writing and deals with everything that happens in the lab. The graduate students Yuan Dai, Tingli Yang, Jian Yang, Ming Wang, and Xin Yi; we worked as a team and accomplished the projects together. I also want to thank the past members, Baohui Liu, Huimin Dong, Junli Guo, Ping Gao and Wei Jie for their friendship and support.

Last but not the least, I would thank the Texas A&M University Health Science Center Institute of Bioscience and Technology where I studied and lived for the past five years. All of the people, the animal facility, HR, administrators, physical plant, security; all together, we make the IBT a better place for research as well as for life. I will cherish those precious memories we have together. Thank you all.

NOMENCLATURE

Rnd3	Rho family small GTPase3
ROCK	Rho-associated coiled-coil protein kinase
CVDs	Cardiovascular diseases
TAC	Transverse aortic constriction
HCM	Hypertrophic cardiomyopathy
DCM	Dilated cardiomyopathy
RCM	Restrictive cardiomyopathy
ARVC	Arrhythmogenic right ventricular cardiomyopathy
IVS	Interventricular septum thickness
LVID	Left ventricle inner dimension
LVPW	Left ventricle posterior wall thickness
EF	Ejection fraction
FS	Fractional shortening
LW	Lung weight
BW	Body weight
TL	Tibia length
Casp3	Caspase 3
GAPDH	Glyceraldehyde 3-phosphate dehydrogenase
MYPT1	Myosin phosphatase target subunit 1
MLC2	Myosin light chain 2

DKO	Double-knockout
VEGF	Vascular endothelial growth factor
HIF1α	Hypoxia-inducible factor 1 α subunit
HRE	Hypoxia responsive element
PHD	Prolyl hydroxylase
HUVECs	Human umbilical vein endothelial cells
CFR	Coronary flow reserve
UPS	Ubiquitin-proteasome system

TABLE OF CONTENTS

Page

Page

Page

LIST OF FIGURES

Page

LIST OF TABLES

Page

CHAPTER I

INTRODUCTION

Cardiovascular Diseases (CVDs)

Cardiovascular diseases (CVDs) including hypertension (high blood pressure, HBP), coronary heart disease, stroke and heart failure have been the biggest threats to the health of Americans. According to the newest data of mortalities statistically summarized by the American Heart Association, CVDs accounted for 31.9% of all deaths in the United States in 2010[1, 2]. Also in 2010, 77.9 million US adults (33% of the entire population) were estimated to have hypertension and the mortality of this disease was 18.8%. Around 15.4 million US adults have coronary heart diseases including heart attack, chest pain, heart failure, stroke and congenital cardiovascular defects. The estimated total cost of treatment for CVDs in 2010 was $315.4 billion. Compared to the estimated $201.5 billion treatment cost of all cancers and benign neoplasms in 2008, CVDs cost much more than any other disease group[1].

Many mechanisms contribute to the development of CVDs. Heart remodeling, vascular remodeling, cardiac cell apoptosis, reactive oxygen species overproduction, energy generation/demand imbalance and disturbed calcium homeostasis could all result in cardiac and vascular dysfunction as well as morphology remodeling. Our lab has been focusing on chronic stimuli caused heart failure in adults and its pathogenesis in response to hemodynamic stress.

Classification of Cardiomyopathies

A cardiomyopathy is characterized as heart muscle disease with an impaired contractile ability or an irregular heartbeat. The prior classification of cardiomyopathies was defined by the 1995 World Health Organization/ International Society and Federation of Cardiology Task Force (WHO/ISFC). It simply identified hypertrophic cardiomyopathy (HCM), dilated cardiomyopathy (DCM), restrictive cardiomyopathy (RCM), arrhythmogenic right ventricular cardiomyopathy (ARVC) and specific cardiomyopathy (unclassified), which made the classification controversial and confusing by mixing the anatomic definition with functional ones[3]. However, it was helpful in understanding the distinctions between the complex diseases. The European Society of Cardiology further made a contemporary classification determined by morphological and functional phenotypes. Based on the cardiomyopathies (HCM, DCM, RCM, ARVC and unclassified cardiomyopathies) defined by the 1995 WHO/ISFC, each cardiomyopathy was further divided into the genetic group and the non-genetic group according to if the cardiomyopathy is caused by genetic polymorphism or not[4]. Debatably, the American Heart Association provided a more complicated classification method depending on the predominant organ involvement and divided the cardiomyopathies into two major categories: primary cardiomyopathies and secondary cardiomyopathies[5]. The primary cardiomyopathies are predominantly confined to heart muscle. They are further divided into genetic, non-genetic and acquired groups. For example, HCM and ARVC/D belong to the genetic group since disease-causing gene mutations are associated in all HCM and ARVC/D patients; while DCM belongs to the genetic/non-genetic mix group. DNA

sequencing became an effective tool in systemically predicting genetic cardiomyopathies. The secondary cardiomyopathies are caused by other pathological factors not predominantly in heart, such as toxicity, inflammation, autoimmune, endocrine and consequences of cancer therapy. Same as the primary category, the secondary cardiomyopathies also can emerge from genetic and non-genetic origins[5].

Hypertrophic Cardiomyopathy (HCM)

Hypertrophic cardiomyopathy (HCM) is an inherited pathological myocardium with hypertrophic remodeling mainly happening in the left ventricle posterior wall, and in certain cases, in the apex, septum, and right ventricle, resulting in an increase in the wall thickness. Patients diagnosed with HCM develop abnormal left ventricular wall thickness ranging widely from 13 to 50 mm[6, 7, 8], and probably in the presence of diastolic dysfunction and other morphological abnormalities such as microvascular disorders, cardiac fibrosis and mitral-valve enlargement or elongation. ECG measurement followed by image detection, including 2-D echocardiography and cardiac MRI analysis, are used for clinical diagnosis. Symmetrical left ventricular hypertrophy is rarely observed, while approximately 50% of patients develop asymmetrical HCM with diffuse left ventricle wall thickening[8].

HCM is a genetic cardiac disease normally associated with the mutation of genes encoding the component proteins of sarcomeres. More than 1600 predominant mutations of 11 genes were identified in the HCM-inherited patients in past decades. The identified

genes encode the proteins that compose the contractile unit of the myofilament or z-disc, such as α-myosin heavy chain, β-myosin heavy chain, troponin T, myosin-binding protein C, vinculin and junctophilin2, and the regulator of myosin such as Rho kinase[8]. However, people with these gene mutations probably do not display a left ventricular hypertrophic phenotype at a young age, but the symptoms might be recognized at adulthood or even at an older age[9]. Therefore, the age-related hypertrophic phenotype development makes the disease difficult to diagnose at an early stage based on the imaging system, while the DNA-based analysis largely facilitates early diagnosis for patients at risk of genetic HCM.

Dilated Cardiomyopathy (DCM)

Dilated cardiomyopathy (DCM) is the heart muscle disease characterized by systolic dysfunction, enlargement of the ventricular chamber and either a normal or thin ventricular wall along with myocyte hypertrophy or elongation. The symptom of DCM can be identified by ECG and 2-D echocardiography, and might be confirmed by an endomyocardial biopsy and coronary angiography. The DNA-based test also facilitates the diagnosis of the genetic defect that causes DCM. Determined by 2-D echocardiography measurement, two important clinical criteria for DCM diagnosis are a 117% or more increase in the left ventricular end diastolic dimension (LVEDD) value and a value of the fractional shortening (FS) less than 25%[10]. In certain cases DCM is diagnosed in the presence of arrhythmias, fibrosis, dynamic obstruction or heart failure.

25%-35% of DCM patients are diagnosed with familial DCM caused by gene mutations, and the remaining patients have the secondary DCM caused by other diseases or conditions[10]. The mutation of the genes encoding the myofilament component protein, the skeleton-plasma membrane network component protein and the calcium channel result in primary DCM, which is a genetic disease and could be inherited by family members. The secondary DCM could be induced by ischemic heart disease, coronary artery disease, hypertension, myocarditis, diabetes, excessive alcohol intake, etc. Our lab has successfully generated the mouse DCM model by the transverse aortic constriction (TAC) technique. Under hemodynamic stress conditions, the mouse heart developed DCM with diastolic and systolic dysfunction, cardiomyocyte apoptosis and capillary rarefaction. This animal model specifically recapitulates the clinical pathological DCM remodeling during the transition of the heart to failure, and is suitable for the mechanistic investigation of DCM etiology.

Rho-associated Coiled-coil Kinase (ROCK) in Physiology and Pathology

Rho-associated coiled-coil kinase (ROCK) was first identified from bovine brain in 1996, and was also named Rho kinase because of its characteristic interaction with GTPγs, RhoA, RhoB and RhoC[11, 12, 13]. As a major downstream effector of RhoA, ROCK is involved in the functions of the Rho family including appropriate responses of extracellular signals, stimulated cytoskeleton dynamics and focal adhesion formation. The two members of the human ROCK family, ROCK1 (ROKβ or p160ROCK) and ROCK2 (ROKα), share 60.9% nucleotide sequence homology and a particularly high

homology of 92% in kinase domains[14], suggesting potential complementary functions between the two isoforms. Both ROCKs are composed of an N-terminal functional kinase domain, a coiled-coil forming region containing Rho-binding domain, a pleckstrin homology (PH) domain and a C-terminal cysteine-rich zinc finger[14].

The ROCK family belongs to the classical serine/threonine kinases PKA, PKG and PKC family[15] and directly or indirectly phosphorylates several downstream targets resulting in the regulation of cytoskeleton dynamics and stress fiber contractility. Myosin light chain (MLC) is one of the substrates phosphorylated by ROCK. The MLC is activated by phosphorylation and directly results in smooth muscle contraction via the facilitation of myosin ATPase[16]. The MLC phosphorylation level is also increased by the inhibition of myosin phosphatase through the phosphorylation modification on its myosin-binding subunit (MBS) by ROCK[17, 18]. ROCK also regulates the formation of stress fibers, focal adhesions and membrane blebs by phosphorylation of LIM-kinase 1 (LIMK1) at threonine 508[19, 20] and LIM-kinase 2 (LIMK 2) at threonine 505[21, 22]. The therefore activated LIMKs phosphorylate and consequently inhibit Cofilin activity which suppresses actin depolymerization and facilitates actin reorganization and stabilization. ROCK also phosphorylates the membrane skeletal proteins Adducin and Ezrin/Radixin/Moesin (ERM) and therefore facilitates the assembly of actin meshwork interaction with the plasma membrane[23, 24]. The ROCK/MLC pathway and ROCK/LIMK/Cofilin pathway-mediated actin-myosin system not only regulate cellular adhesion, motility, morphology and intracellular transportation, but also play a

regulatory role in smooth muscle cell calcium sensitivity[25] and the apoptotic cell membrane blebbing process[26].

Due to the important roles of ROCK in cytoskeleton-dependent cellular processes, ROCK was found as a key factor in oncogenesis. ROCK has been implicated in proliferation, invasion and metastatic growth of multiple cancer cells[27, 28].

ROCK, a Key Modulator in Cardiovascular Diseases

ROCK inhibitors Fasudil and Y-27632 were developed for the research of ROCK's function in diseases and the therapeutic effects. Both two chemicals target the ATP-dependent kinase domain of ROCK, and therefore have potential non-selective effects on other kinases such as PKA and PKC at high concentrations[15]. Fasudil is the only currently approved ROCK inhibitor for human use, which has been applied on the clinical treatment of cerebral vasospasm in Japan. The ROCK inhibitors were used in multiple animal models *in vivo* and cell experiments *in vitro* to study the functions of ROCK and the underlining mechanisms in cardiovascular diseases.

The effects of ROCK on vascular smooth muscle cells have been extensively studied. ROCK promotes smooth muscle cell contraction[29], migration[30] and proliferation[31, 32], which contribute to hypertension development. Activation of ROCK has been detected in many hypertension animal models and hypertensive patients. Application of Fasudil in spontaneously hypertensive rats (SHR) effectively suppressed smooth muscle cell

contraction and calcium sensitivity mediated high blood pressure, meanwhile hypertensive blood vessel lesion formation, vascular hypertrophy and fibrosis were reduced with long-term Fasudil treatment[33]. Fasudil induced the activation of MLC phosphatase (MYPT1) and the decrease in MLC phosphorylation levels suppress the mean arterial blood pressure in the SHR mouse model[33, 34].

ROCK has been implicated in the regulation of endothelial cell migration and endothelial monolayer permeability[35, 36, 37]. Stimulated by vascular endothelial growth factor (VEGF) and shear stress, the RhoA/ROCK pathway is activated and promotes endothelial cell migration and angiogenesis[35, 38]. The anti-cancer drug vinca alkaloids can lead to pulmonary edema in breast cancer patients due to endothelial barrier dysfunction[39]. The phosphorylation of MYPT1 and LIMK by ROCK results in microtubule destabilization in endothelial cells and was suggested as the mechanism[36, 37]. Furthermore, ROCK induces the decrease of eNOS and phosphorylated eNOS levels, and therefore results in reduced NO production and endothelial dysfunction[34].

Atherosclerosis is characterized by endothelial hyper-permeability, inflammatory cell recruitment and lipoprotein accumulation which can be mediated by ROCK signaling. Haploinsufficient ROCK1$^{+/-}$ mice underwent carotid artery ligation induced vascular injury, and developed reduced neointima formation and bone marrow-derived leukocyte infiltration compared with that of WT or ROCK2$^{+/-}$ mice, indicating that ROCK1 plays an essential role in inflammatory atherosclerosis plaque development[40]. Studies also

showed that ROCK regulated the early development of atherosclerosis via NF-κB activation and T lymphocyte accumulation[41].

ROCK pathway activation was observed in multiple cardiac hypertrophy and ventricular remodeling animal models as well as in heart failure patients. Our lab previously reported that after one week of hemodynamic stress exposure ROCK1$^{-/-}$ mouse myocardium displayed a significantly reduced number of apoptotic cardiomyocytes compared with that of WT mice. ROCK1 can be cleaved and consequently activated by caspase 3, meanwhile the truncated ROCK1 facilitates caspase 3 activation which forms a feed-back regulatory loop to promote apoptosis[42]. The transgenic mouse line overexpressing truncated ROCKΔ1, which is the constitutively active form of ROCK1, was generated by our group. By infusion of angiotensin-II, the ROCKΔ1 transgenic mice developed severe fibrotic cardiacmyopathy associated with cardiac dysfunction. In the ROCKΔ1 heart, ROCK1 positively modulated the TGFβ1 and NF-κB pathway in a serum response factor (SRF)-dependent manner, which is responsible for the differentiation of cardiac fibroblasts into myofibroblasts[43].

Endogenous Regulators of ROCK

The Rho-binding domain and PH domain located at the C-terminal of ROCK is a negative regulatory region leading to conformational autoinhibition. The cleavage of the ROCK1 C-terminal by caspase 3 in apoptosis generates a constitutively active form, while this process is not present in ROCK2[26, 44]. Binding of the Rho family, including

RhoA, RhoB and RhoC, to the Rho-binding domain of ROCK can also release the catalytic kinase domain and stimulate ATP-dependent kinase activity. As a negative regulator, small GTPase Rnd3 (RhoE) binds to a region encompassing the kinase domain of ROCK1, leading to the inhibition of ROCK1 and the conformational competition with the binding of RhoA to ROCK1 although there is a distance between the two binding sites[45, 46, 47]. PDK1 competes with Rnd3 for binding to ROCK1 resulting in ROCK1 translocation to the plasma membrane and reduced kinase activity[48]. Considering the multiple regulatory roles of ROCK1 in cardiovascular diseases, I focused on the study of its inhibitor, Rnd3, and its function in the heart.

ROCK 1 Endogenous Inhibitor: Rnd3 in Physiology and Pathology

The Rho family proteins belong to the Ras superfamily of GTPases. Best characterized Rho family proteins include Rho, Rac and Cdc42. Recently, study of the Rnd subfamily, Rnd1, Rnd2, Rnd3/RhoE, which are expressed widely across vertebrates, is becoming interesting. Rnd3 is the first identified member of the Rnd subfamily, discovered by Jeffrey Settleman's lab while studying its ability to interact with p190RhoGAP[49]. Unlike the well characterized small GTPase, such as RhoA, Rnd3 binds to GTP but lacks intrinsic GTPase activity and is resistant to Rho-specific GTPase-activating proteins.

Rnd3 expression is regulated by many different stimuli. DNA damage caused by chemotherapeutic agents or UV irradiation up-regulated Rnd3 expression in both mRNA and protein levels. The response to chemotherapeutic agents is believed to be associated

with p53[46, 50], while the UV-mediated up-regulation of Rnd3 in keratinocytes is independent of p53[51]. Other regulators have been shown to be involved in the regulation of Rnd3 expression in cancers. Rnd3 expression is related to NF-κB activity in prostate cancer[52]; the mTOR pathway is closely associated with Rnd3 expression in subependymal giant cells in brain tumors[53]. Moreover, microRNA may regulate Rnd3 expression. Rnd3 was identified as a potential miR-200c target gene by using the informatics and q-PCR method[54]. At the posttranslational level, Rnd3 can be stabilized by ROCK1&PKC phosphorylation[55, 56]. Recently one study showed that Rnd3 can physically interact with 14-3-3 to regulate its membrane localization, which provides a new mechanism for the investigation of Rnd3 regulation[57].

Biological function of Rnd3 has been studied in cultured cell lines predominantly. Rnd3 decreases actomyosin contractility, and induces loss of stress fibers *in vitro*[58]. In smooth muscle cells, the Rnd3-mediated decrease in cell contractility is proposed to be critical in preventing contraction of the myometrium in pregnant rabbits[59, 60]. Rnd3 is an endogenous inhibitor of ROCK1[45]. It binds to ROCK1 to inhibit phosphorylation of other ROCK1 downstream targets, such as myosin light chain phosphatase (MYPT1). In cancer, Rnd3 has both pro- and anti- cancer cell migration effects depending on different cell types. Rnd3 is down-regulated in aggressive prostate cancers[61], while it promotes melanoma cell invasion, and is highly expressed in colon cancer cells and pancreatic tumors[62, 63, 64]. In the brain, recent studies found that Rnd3 was indispensable in mouse neuron development through the Rho kinase-dependent signaling pathway[65, 66, 67].

Genetic deletion of *Rnd3* in the mouse was established in our lab. My study suggests that loss of Rnd3 results in aqueduct stenosis leading to hydrocephalus through up-regulation of Notch signaling[68].

Study of Rnd3 in Heart

The biological function of Rnd3 in the heart remains unexplored. One microarray screening study showed a significant decrease in the Rnd3 mRNA levels in failing human myocardia (Profile GDS651/212724_at/RND3 in NCBI GEO profiles). The etiologic meaning of Rnd3 down-regulation in the human failing heart is unknown, therefore the investigation of Rnd3 in the heart has clinical significance. In order to study the pathological meaning of Rnd3 down-regulation in human heart diseases, our lab generated Rnd3 knockout mice, which provided a novel mouse model to address the proposed question.

Our lab recently found that the Rnd3-null mice died at the early stage of E11 with heart failure and fetal arrhythmias. Ca^{2+} leakage due to the ryanodine receptor type 2 (RyR2) Ca^{2+} release channels destabilization was detected in embryonic $Rnd3^{-/-}$ cardiomyocytes. The Rnd3 deficiency mediated PKA signaling activation was suggested to contribute to the impaired Ca^{2+} homeostasis[69]. Rnd3's pathological function in the adult heart would be our future research emphasis.

Cardiac Angiogenesis and Heart Disease

Angiogenesis and vasculogenesis are two major processes involved in vasculature development and pathological remodeling. The former is characterized by vessels sprouting from an existing vascular structure, while the latter is the early stage process that vessels develop from bone marrow derived endothelial progenitors. Many steps have been implicated in angiogenesis: degradation of matrix around endothelium, migration and proliferation of endothelial cells, 3-dimentional vessel formation by endothelial cells, migration of smooth muscle cells and pericytes to form a mature vessel.

Angiogenesis plays an important role in heart remodeling as an adaptive response to the increased demand of oxygen, nutrient and chemokine transportation. In response to physiological stimuli, such as the transition from the postnatal to the adult heart, cardiac growth occurs predominantly through a hypertrophic process[70]. This postnatal cardiac hypertrophy is accompanied by a proportional growth of myocardial vasculature[71]. In aerobic exercise, the heart develops physiological hypertrophy along with a corresponding growth in coronary microvessels[72, 73]. Besides the physiological stimuli, many pathological stimuli such as shear stress, pressure overload, hypoxia and inflammation are known to promote cardiac angiogenesis[74, 75]. However, the compensatory enhancement of angiogenesis in response to these pathological stimuli appears to be insufficient, and this insufficiency is one of the critical factors responsible for the transition of the heart from compensated hypertrophy to heart failure[76, 77]. Various chemokines and angiogenic growth factors including vascular endothelial

growth factor (VEGF)[78, 79], fibroblast growth factor (FGF)[80], angiopoietin (Ang)[81], endothelin 1 (ET-1)[82, 83, 84], transforming growth factor-β (TGF-β)[85] and NF-κB[86] are considered to be involved in regulating the angiogenesis process.

Based on the mechanistic study of angiogenesis, the application of pro-angiogenic growth factors in heart ischemia rescue and cardiac function improvement has become a promising therapeutic strategy. Pro-angiogenic factors such as VEGF and FGF have been compensated in myocardial ischemia treatment in many animal studies and clinical trials by delivering naked DNA, adenovirus or retrovirus and direct injection of recombinant protein. The angiogenic factor administrations have succeeded in animal studies[87, 88, 89, 90], however do not work well in clinical trials. In phase 1 studies, patients with under-perfused myocardium received a recombinant VEGF (rhVEGF) protein intracoronary injection. The clinical results showed that collateral density was increased and myocardial perfusion was improved by rhVEGF administration[91, 92]. In the phase II VIVA (Vascular endothelial growth factor in Ischemia for Vascular Angiogenesis) trial 178 patients randomly received rhVEGF or a placebo by intracoronary infusion and both groups displayed improved exercise tolerance and myocardial perfusion at the endpoint, however, without a significant difference[93]. The mechanism underlying the discrepancy between the preclinical animal studies and practical therapeutic angiogenesis is still not known.

VEGFs in Angiogenesis Regulation

VEGF family is one of the predominant pro-angiogenic factors regulating angiogenesis. The VEGF family contains 7 members: VEGFA (or VEGF1), VEGFB (or VEGF2), VEGFC (or VEGF3), VEGFD, VEGFE, VEGFF and placental growth factor (PlGF). Encoded by *VEGF* gene, different splicing isoforms were found in human: $VEGF_{121}$, $VEGF_{145}$, $VEGF_{165}$, $VEGF_{189}$ and $VEGF_{206}$. The VEGFs selectively bind to specific tyrosine kinase receptors (VEGFR1, VEGFR2 and VEGFR3), which are facilitated by co-receptors neuropilin1 and neuropilin2[94]. VEGFR1 (or flt-1) and VEGFR2 (or KDR, flk-1) are majorly expressed in endothelium, and can be activated by the binding of VEGFA, VEGFB, VEGFC and VEGFD[95, 96]. VEGFR3 (or flt-4) is majorly expressed in adult lymphatic endothelium, and functionally restricted to lymphagiogenesis through the binding with its ligands VEGFC and VEGFD.

VEGFA is the first discovered VEGF family member, therefore in the earliest study, VEGFA was reported as VEGF. The VEGFR2 mediated VEGFA signaling is identified as the most important and dominant regulator of angiogenesis and vasculogenesis[97]. Deletion of a single VEGFA allele causes embryonic lethality and abnormal vessel development[78, 79]. VEGFA has been implicated in promoting endothelial cell survive and proliferation, endothelial progenitor cell recruitment, stimulating new vessel formation, and in tumor angiogenesis inducing vascular permeability and vasodilation[97, 98, 99, 100]. The up-regulation of VEGFA was found in ischemic animal hearts[101, 102, 103] and acute myocardial infarction patients, indicating that VEGFA might be an ischemia induced

angiogenic factor. As a major source of VEGFA in the heart, cardiomyocytes secrete VEGFA in response to hypoxia and hemodynamic stress. A transcription factor hypoxia-inducible factor 1 (HIF1α) takes major responsibility for VEGFA expression in the hypoxia region[104]. In a recent study, a hypoxia-independent pathway regulating VEGFA expression by PGC-1α was reported[105].

Hypoxia-inducible Factor 1α (HIF1α), a Key Regulator of VEGFA

Hypoxia-inducible factor (HIF) is a dimer transcription factor composed of α and β subunits. The HIFβ subunit is constitutively expressed nuclear protein while the HIFα subunit is dynamically regulated and functions in an oxygen-sensitive pattern[104]. The transcription of HIFα is barely regulated, whereas HIFα can be regulated at the post-translational level[106]. In full oxygenation condition, HIFα is dually regulated through two different mechanisms. HIF prolyl hydroxylases 1-3 (PHD1-3) make hydroxylation modifications on HIFα at the prolyl residues (Pro), resulting in the recruitment of E3 ubiquitin ligase von Hippel-Lindau (VHL) and undergoing the proteasome degradation[107, 108]. HIFα also can be hydroxylated at asparaginyl residue (Asn) in the C-terminal (C-TAD) by HIF asparaginly hydroxylase (FIH). This modification on Asn803 residue impedes the interaction of HIFα with co-activator p300 in the nucleus resulting in repressed transcriptional activity[109]. In hypoxia condition, the activity of PHD and FIH are repressed consequently stabilizing HIFα protein, suggesting that PHD and FIH are cellular oxygen sensors modulating HIFα mediated hypoxia response signaling in an oxygen-dependent manner[110].

Three isoforms (HIF1α, HIF2α, and HIF3α) are included in the HIFα family. The HIF1α and HIF2α share a 48% identity in amino acid sequence and therefore share a similar structure and regulation mechanism. To initiate transcriptional activity, both HIF1α and HIF2α can translocate from the cytoplasm to the nucleus, forming a heterodimer with HIF1β[106]. The co-activator p300 and CREB binding protein (CBP) facilitate the affinity of the HIF heterodimer with the DNA motif hypoxia responsive elements (HREs)[111, 112].

The downstream target genes are involved in many signaling pathways including promoting oxygen delivery (angiogenesis), and inhibiting oxygen consumption (glycolysis, lipid metabolism and NO production). VEGFA is one of the most important target genes in the regulation of hypoxia induced angiogenesis in cardiac adaptive response and tumor growth. Both HIF1α and HIF2α directly regulate VEGFA expression in some cell types such as renal carcinoma cells and Hep3B cells. However, HIF1α, but not HIF2α, uniquely activates VEGFA expression in mouse embryonic cells, indicating that HIF1α is the more potent and dominant regulator of VEGFA[113, 114, 115, 116, 117].

CHAPTER II

MATERIALS AND METHODS

Source of Human Myocardium

51 human failing heart samples were obtained from the end-stage heart failure patients at the time of transplantation. All heart failure patients have severe impaired cardiac function with <20% left ventricular ejection fraction. 12 human normal myocardial samples were obtained from the patients died of non-cardiac causes. The Institutional Review Board of Methodist Hospital approved all protocols.

Generation of Rnd3 Knockout (KO) and Rnd3/Rock1 Double Knockout (DKO) Mouse Lines

Rnd3 knockout mouse line was derived from a gene trap ES cell line from Texas Institute for Genomic Medicine (TIGM). A targeting vector carrying a lacZ expressing cassette was inserted into intron 2 of *Rnd3* gene. The *Rnd3* mutant allele was identified by PCR using the primers (5' to 3'): A148a: TCCATAGAGGGTAAAGCCATCC / A148b: AAAGGTACTCCCAGAGAGCTAAGG;

A148a: TCCATAGAGGGTAAAGCCATCC / A148c: ATAAACCCTCTTGCAGTTGCATC. The *Rnd3* knockout allele was also confirmed by Southern Blotting[69]. The Rnd3-null mice were lethal at E11.5 stage, therefore Rnd3 haploinsufficient mice were used for mouse line maintenance.

The establishment of ROCK1 knockout mouse line was described previously[68]. I generated $Rnd3^{+/-/ROCK1-/-}$ mouse line (DKO) by breeding $Rnd3^{+/-}$ with $ROCK1^{-/-}$ mice. All animal experiments were approved by the Institutional Animal Care and Use Committee of the Texas A&M University Health Science Center.

Mice Work, Fasudil Treatment and Cobalt Chloride ($CoCl_2$) Treatment

Mice were treated with 1mg/mL Fasudil (LC Laboratories, MA, USA) in drinking water for 3 weeks immediately after TAC surgery. Mice were treated with 2mM cobalt chloride (Alfa Aesar, 12303, MA, USA) in drinking water for 3 weeks immediately after TAC surgery. All animal experiments were approved by the Institutional Animal Care and Use Committee of the Texas A&M University Health Science Center.

Cardiac Function Assessment by Echocardiography

Cardiac functions were measured using a Vevo770 High-Resolution *In Vivo* Micro-Imaging System (VisualSonics, Toronto, ON, Canada) with a RMV-707B probe. 10-15 weeks old male mice were anesthetized with 3% isoflurane mixed with 100% oxygen, then followed by the anesthetization with 1-1.5% isoflurane. After the mice heart rate decreased to 380-420 beats per min, the 2-D echocardiography of anterior (+septum) and posterior walls were recorded at the papillary muscles level.

Transverse Aortic Constriction (TAC)

10-15 weeks old adult male mice were anesthetized with 3% isoflurane mixed with 100% oxygen. After the thymus was retracted and the transverse aorta was exposed, a 3mm length of 27 gauge needle was put besides the aorta between the right innominate and left carotid artery. The aortic constriction was performed by tying a 6-0 suture against the needle. By removing the needle after two knots the constriction was achieved. The procedure yielded a 60%-80% constriction on transverse aorta diameter. After the surgery, the artery flow velocity was measured by Doppler (Indus Instruments, Houston, USA), and the ratio of right-to-left carotid artery flow velocity was calculated. To minimize surgery variation, the mice with the ratio between 5 and 10 were used for further experiments. Sham group without occlusion served as a control. All TAC surgery induced pressure overload lasted for 3 weeks.

Blood Pressure Assessment

Mouse was trained for 3 days until it stayed quiet in the animal holder of Mouse Blood Pressure System (MRBP-MMC, IITC Life Science Inc, CA, USA). Systolic blood pressure was assessed through tail cuff method, and diastolic blood pressure was calculated by software MRBP Monitor Version 1.59.

Coronary Flow Reserve Assessment by Doppler

Mouse coronary flow reserve was measured using MM3 system (World Precision Instruments, FL, USA) with a Pulsed Doppler probe (Indus Instruments, TX, USA). The

method was modified from George E. Taffet's lab[118]. 10-15 weeks old male mice were anesthetized with 2% isoflurane mixed with 100% oxygen, then followed by the anesthetization with 2.5% isoflurane (hyperemic condition) and 1% isoflurane (basal condition), respectively. The peak flow velocities in left main coronary were recorded under the hyperemic condition and the basal condition, respectively. The ratio of hyperemic over basal coronary velocity was considered as the index of coronary flow reserve.

Hematoxylin and Eosin Staining, Immunostaining and Immunoblotting

Mice hearts were perfused and fixed by Langendorff Perfusion System (Radnoti, 120108). The whole heart paraffin sections were applied to Hematoxylin and Eosin Staining (51275, Fluka; HT110132-1L, Sigma-Aldrich) and terminal deoxynucleotidyl transferase dUTP nick end labeling (TUNEL) staining (In situ cell death detection kit, 11684795910, Roche, USA). Phalloidin staining (A12381, Invitrogen, USA) and DAPI staining were used to label F-actin and nuclei, respectively. Isolectin GS-IB4 staining (I21411, Invitrogen, NY, USA) was used to visualize capillaries. For each heart sample, images from 5 fields were acquired by Leica DM2000 fluorescence microscopy (Leica Microsystems Inc., IL, USA). One image was from the top of interventricular septum and four images were from the left ventricle wall. The images for TUNEL staining results were quantified by Leica Application Suite Imaging Software (Version 4.0, Germany).

Protein samples for immunoblotting were extracted and separated from mice hearts as described previously[119]. Antibodies from the following sources: Caspase-3 (sc-7148) from Santa Cruz Biotechnology (CA, USA); MLC2 (PA5-17624), Phospho-Thr18/Ser19 MLC (PA5-17727) from Thermo Scientific Pierce (IL, USA); MYPT1 (2634S), Phospho-T853 MYPT1 (4563S) from Cell Signaling Technology (MA, USA); c-Myc (sc-40) and HA (sc-805) from Santa Cruz Biotechnology (CA, USA); VEGF (ab1316) from abcam (MA, USA); HIF-1 alpha (H1alpha67) from Novus Biologicals (CO, USA) are commercially available. Rnd3 antibody was made from Cocalico Biologicals (PA, USA). Protein loading was normalized by the GAPDH (Santa Cruz, sc-20357) blotting intensity.

Hypoxyprobe-1 Staining

For *in vivo* hypoxia region detection, HP1-100Kit was used (Hypoxyprobe Inc, MA, USA). Mice were intraperitoneal injected 80mg/kg Hypoxyprobe^{TM}-1, and sacrificed 60 min later. The Hypoxyprobe^{TM}-1 deposited at hypoxia region. Hearts were harvested and processed for paraffin embedding. Anti-mouse IgG (MAb1, Hypoxyprobe Inc, MA, USA) immunostaining was performed to detect the Hypoxyprobe^{TM}-1 in cardiac sections.

Cardiomycyte Isolation

10-15 week-old adult male mouse was sacrificed, and the heart was harvested and transferred to perfusion buffer immediately. Transverse aorta was cannulated by a 22 G cannula, and was tied to the cannula before the cannula tip reached aortic valve. Then

the heart was uploaded to Langendorff Perfusion System (120108, Radnoti, CA, USA) for the following enzyme digestion. Briefly, the heart was continually perfused at 37°C by the digestion buffer containing 0.15 mg/mL Liberase TM (05401127001, Roche, IN, USA). The digestion process lasted 8-10 min. After digestion, the heart became swelled and soft. The digestion was terminated by 5% fetal bovine serum (FBS) and cardiomyocytes were carefully dissociated. After calcium reintroduction, the cardiomyocytes were seeded onto laminin-coated dishes. MEM medium containing 5% FBS was used for the cardiomyocyte culture. After the cells were cultured for 16 hours, the conditional medium was collected for the following HUVECs tube formation assay and ELISA assay.

Tube Formation Assay, Cell Culture, Hypoxia Treatment and Gene Transient Transfection

Human umbilical vein endothelial cells (HUVECs) were cultured in EGM medium (CC-3162, Lonza, NJ, USA) for 24 hours in advance to the tube formation assay. Then the HUVECs were trypsinized and seeded onto BME gel (3433-005-01, Trevigen, MD, USA) coated dishes with non-growth factor EBM medium (CC-3156, Lonza, NJ, USA). After the cell attachment, the EBM medium was replaced by the cardiomyocyte conditional medium for the following HUVECs tube formation process. The tube structures were matured after 6 hours. Images were acquired under 5 x magnifications, and analyzed by WimTube Image Analysis software (ibidi GmbH, Germany).

Hela cell line was cultured in DMEM medium containing 10% FBS for *in vitro* experiments, including luciferases assay and immunoprecipitation.

For hypoxia treatment, cell culture dishes were put into hypoxic condition chamber (MIC-101, Billups-Rothenberg Inc, CA, USA). The cells were cultured in 1% O_2 for 16 hours.

siRNA specific for human RND3 knockdown was purchased from Thermo Scientific (L-007794-00-0050). Expression construct human HA-HIF1alpha-pcDNA3 (plasmid#18949) was purchased from Addgene; construct GST-Rnd3 was generated with pGEX-6P-1 backbone (GE Healthcare); construct myc-Rnd3 was generated as described previously[68].

VEGFA Measurement

VEGFA protein level in cardiomyocyte conditional medium was assessed by the commercially available VEGF Mouse ELISA Kit (ab100751, abcam, MA, USA). The whole process included the following multiple steps. 1. Sample preparation: WT and $Rnd3^{+/-}$ cardiomyocyte conditional medium were harvested after 16h-cell culture, and the supernatant was collected after centrifuge. The supernatant was ready for VEGFA measurement. 2. Sample loading: VEGFA standards were prepared as the manufacture described. The supernatant from the medium was diluted by 4 folds. The standards and the samples were loaded to the 96-well plate which had been coated with VEGFA

primary antibody. Duplicate loadings were applied to minimize variance. 3. Measurement: The samples were incubated with the primary antibodies at 4°C for overnight, followed by wash processes. The biotinylated second antibody was incubated with the sample-primary antibody complex in the plate for 1 hour at room temperature. After the immune binding process, the substrate of biotin was added to each well, and the reactions were terminated after 45 min. The optical density was measured by a microplate reader at 450 nm immediately.

QPCR (quantitative polymerase chain reaction) Analysis

Transcripts were quantified by StepOnePlus™ Real-Time PCR Systems (Applied Biosystems, CA, USA) with SYBR Green master mixes buffer system (4367659, life technologies, NY, USA). Total RNAs was extracted by TRIzol (15596-026, life technologies, NY, USA). The forward / reverse QPCR primers (5′ to 3′) were as follows: VEGFA (mouse): CTGTGCAGGCTGCTGTAACG/GTTCCCGAAACCCTGAGGAG; GAPDH (mouse): GAGTCAACGGATTTGGTCGT/TTGATTTTGGAGGGATCTCG.

Luciferase Assay

Luciferase report vector with a VEGFA promoter composed by three HIF1 response elements is commercially available (HRE-luciferase, plasmid #26731, Addgene). Renilla luciferase vector (E1960, Promega) served as a control. Transient transfection of vectors into Hela cell line was described previously[120]. The luciferase assay was performed 36 hours after post-transfection. Cells were lysed by the buffer from Promega (E3971), and

20 of 150 µl lysis supernatant were used for assay. A lumat3 LB9508 luminometer (Berthold) was used to read out optical density. Each sample measurement was triplicated to minimize variance.

Statistical Analysis

Data are presented as means ± s.d. Unpaired, two-tailed student's *t* test was used for two group comparisons. One-way ANOVA followed by Student-Newman-Keuls test was used for multiple group comparisons. Chi-square Fisher's test was used for survival rate statistical analysis. All statistical analyses were performed in software SigmaPlot 11.0 (Systat, San Jose, CA, USA). The P value < 0.05 was considered as significant difference.

CHAPTER III

RESULTS

RND3 is Down-regulated in End-point Stage Human Failing Hearts

The clinical pathological significance of Rnd3 in heart is barely reported. A RNA microarray study from NCBI database has probed the mRNA levels of Rnd3 from normal human hearts, idiopathic dilated failing human hearts and ischemic failing human hearts. Significantly reduced Rnd3 mRNA levels were found in those heart failure patients (Profile GDS651/212724_at/RND3 in NCBI GEO profiles). To explore the RND3 protein expression profile in human pathological hearts, 51 human failing heart samples and 12 normal heart samples were analyzed by RND3 immunoblotting.

In the heart samples from the end-point stage heart failure patients, RND3 protein levels significantly decreased compared with the human normal hearts (Figure 1a). The densitometry of RND3 protein levels were normalized by GAPDH, and the average RND3 level in the failing hearts was down-regulated by 57.9% compared with the normal hearts (Figure 1b).

The down-regulation of RND3 expression in human failing hearts suggested an important modulatory role of RND3 in the etiology of the transition of the heart to failure. To investigate the pathological significance of RND3 down-regulation in human

hearts, Rnd3 knockout mouse line was generated to recapitulate the situation observed in heart failure patients.

Figure 1. RND3 Protein Levels were Down-Regulated in Failing Human Hearts. (a) Representative image for immunoblotting of RND3 and GAPDH in human normal hearts and human failing hearts. (b) Densitometry quantification of RND3 protein levels from 12 human normal hearts and 51 human failing hearts normalized by GAPDH. Unpaired, two-tailed student's *t* test was used for two group comparisons. The P value < 0.05 was considered as significant difference. Data are presented as means ± s.d.

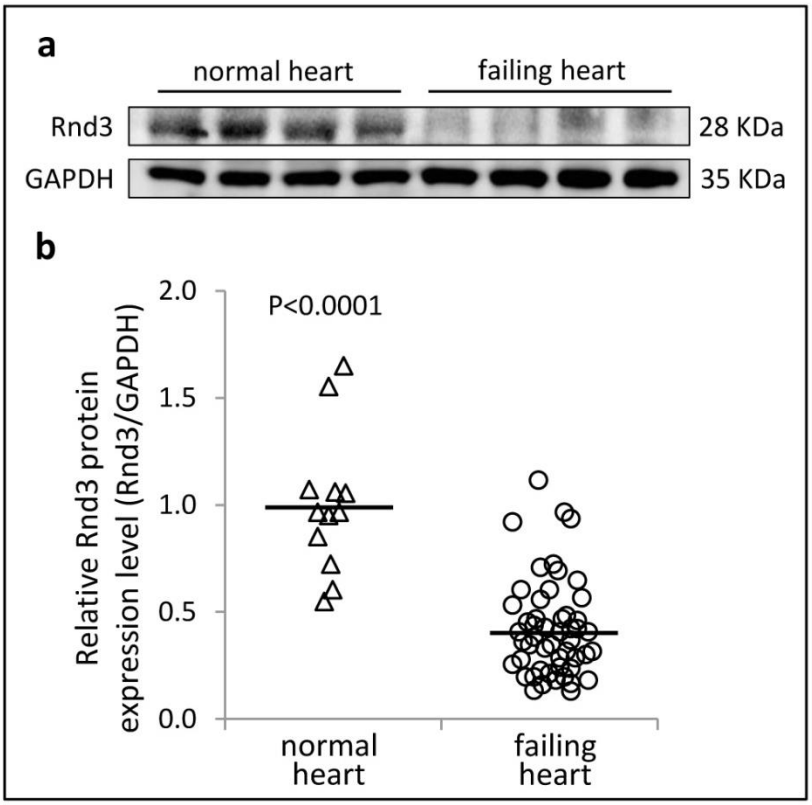

Rnd3$^{+/-}$ Haploinsufficient Mice Displayed Normal Heart Morphology and Cardiac Function

To investigate the Rnd3's function in mouse heart, Rnd3 gene trap knockout mouse line was generated. Rnd3$^{-/-}$ mice were lethal at embryo E11.0 stage associated with heart failure and arrhythmia, however, Rnd3$^{+/-}$ haploinsufficient mice were viable and displayed no abnormal phenotype under physiological condition.

The heart morphology and cardiac function were detected in Rnd3$^{+/-}$ 10-12 weeks old male mice by echocardiography. Based on the doppler signals of live hearts, in Rnd3$^{+/-}$ adult hearts, interventricular septum thickness (IVS), left ventricle inner dimension (LVID) and left ventricle posterior wall thickness (LVPW) showed no difference compared with wild type (WT) hearts (Table 1). The cardiac capability of pumping blood out from ventricle was described by stroke volume, ejection fraction, fractional shortening and cardiac output. The mutant hearts also displayed normal cardiac function compared with the WT hearts (Table 1).

The impaired cardiac function in Rnd3$^{-/-}$ homozygous mouse embryos suggests Rnd3's essential role in the embryonic heart development. However the Rnd3's function in adult heart remodeling was unexplored. Under physiological condition the Rnd3$^{+/-}$ mice exhibited the normal heart phenotype. To investigate the response under pathological condition, a challenge would be performed on these mice.

Table 1. Rnd3$^{+/-}$ Mice Displayed No Abnormality in Heart Morphology and Cardiac Function Compared to Wild-Type (WT) Mice. Echocardiography assessments of heart morphology and cardiac function were performed in 7 pairs of 10-15 weeks-old WT and Rnd3$^{+/-}$ male mice. No significant difference was detected. IVS: interventricular septum thickness; LVID: left ventricle inner dimension; LVPW: left ventricle posterior wall thickness; d: diastolic; s: systolic. Statistical significance was determined by unpaired, two-tailed student's t test. Data are means ± s.d.

Parameter	WT	Rnd3$^{+/-}$
n	7	7
Body weight (g)	25.59±4.02	25.52±2.11
IVS;d (mm)	0.77±0.09	0.75±0.14
LVID;d (mm)	3.83±0.47	4.02±0.41
LVPW;d (mm)	0.67±0.08	0.66±0.13
IVS;s (mm)	1.13±0.06	1.17±0.16
LVID;s (mm)	2.53±0.40	2.65±0.51
LVPW;s (mm)	1.01±0.14	1.05±0.16
Stroke Volume (μl)	42.61±9.53	49.74±8.00
Ejection Fraction (%)	66.11±6.73	66.37±7.57
Fractional Shortening (%)	36.11±4.82	36.63±5.97
Cardiac Output (ml/min)	16.74±4.23	19.44±4.27

Rnd3$^{+/-}$ Mice were Predisposed to Transverse Aortic Constriction (TAC) Induced Hemodynamic Stress and Developed Heart Failure Associated with Dilated Cardiomyopathy Phenotype

The hemodynamic stress induced by transverse aortic constriction (TAC) surgery was broadly used on rodents to generate pressure overload and induce heart remodeling. The

TAC surgery could induce multiple heart diseases including cardiac fibrosis, apoptosis and hypertrophy. These animal models greatly facilitate the research study in cardiology field. According to the echocardiography analysis results, $Rnd3^{+/-}$ mice were viable and exhibited normal cardiac function and morphology at basal condition. To investigate Rnd3's role in pathological heart, the $Rnd3^{+/-}$ mice and WT mice were exposed to TAC stress for 3 weeks.

The whole animal hearts were harvested and morphology changes were observed after TAC surgery. Thick left ventricular posterior wall and enlarged chamber were observed in the WT heart after TAC challenge, indicative of compensatory hypertrophy in response to stress (Figure 2a, WT TAC); however, the $Rnd3^{+/-}$ heart displayed much larger left ventricular chamber and even thinner ventricular wall after TAC, indicative of a dilated cardiomyopathy phenotype (Figure 2a, $Rnd3^{+/-}$ TAC). This typical dilated cardiomyopathy phenotype in the mutant heart after TAC suggested damaged cardiac function. Detected by echocardiography, ejection fraction (EF) and fractional shortening (FS) of the $Rnd3^{+/-}$ mice heart decreased dramatically from 66.7% and 36.8% to 15.1% and 6.7%, respectively, indicating that heart failure happened in the $Rnd3^{+/-}$ mice heart under hemodynamic stress (Figure 2b). Consistent with the echocardiographic results, lung edema was observed (data not shown) and significant increase in lung weight (LW) was detected in the $Rnd3^{+/-}$ mice, which confirmed the heart failure development (Figure 2c).

Figure 2. Rnd3$^{+/-}$ Mice Developed Heart Failure 3 Weeks after Transverse Aortic Constriction (TAC) Surgery. (a) Representative images for whole hearts and Hematoxylin and Eosin stained cardiac sections for wild type (WT) and Rnd3$^{+/-}$ mice before and after TAC surgery. The mutant hearts were enlarged in response to TAC stress. (b) Significant decrease in cardiac function determined by ejection fraction (EF) and fractional shortening (FS) was detected in Rnd3$^{+/-}$ mice comparing with WT mice after TAC. (c) Significant increases in the ratio of lung weight (LW) over body weight (BW) and the ratio of LW over tibia length (TL) were observed in Rnd3$^{+/-}$ mice comparing with WT mice after TAC, indicating heart failure development. The number in each column represents animal numbers in each group. One-way ANOVA followed by Student-Newman-Keuls test was used for multiple group comparisons. The P value < 0.05 was considered as significant difference. Data are presented as means ± s.d. Scale bar represents 1mm.

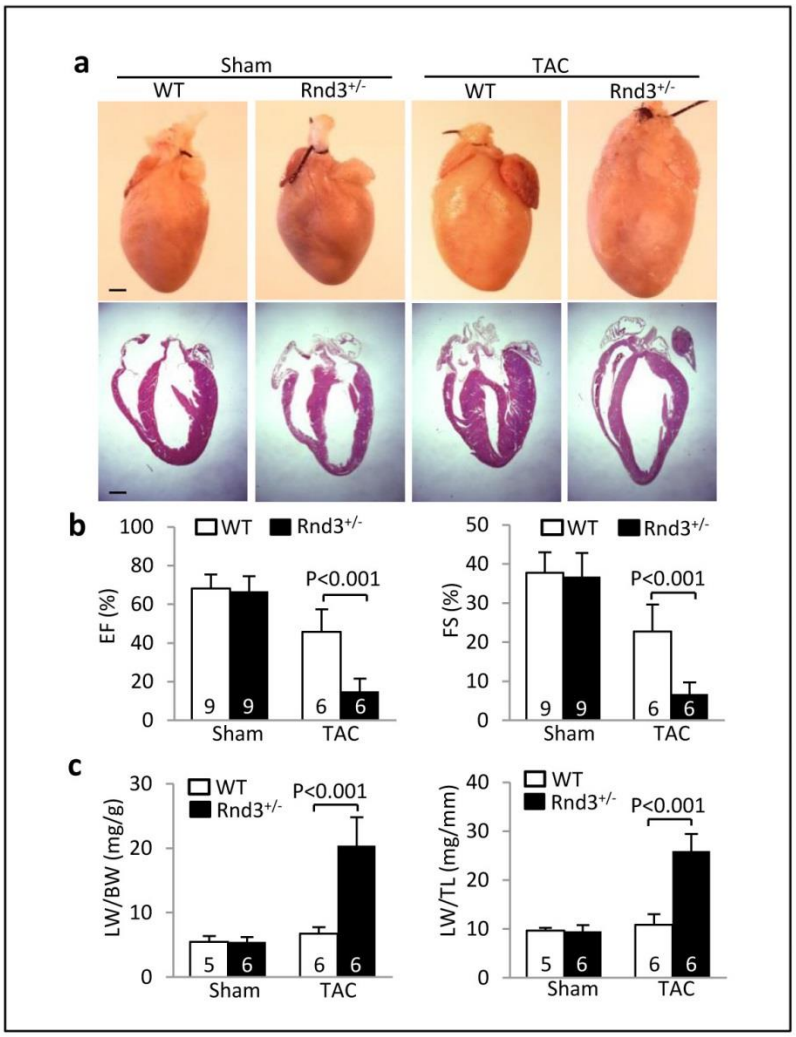

To confirm the cardiac phenotype, left ventricular internal dimension at systole (LVIDs) and left ventricular posterior wall thickness at systole (LVPWs) were assessed via echocardiography (Figure 3a, b). The sham group WT and $Rnd3^{+/-}$ hearts exhibited no significant difference, while after TAC the LVIDs of the $Rnd3^{+/-}$ heart dramatically increased from 2.47 mm to 4.05 mm and the LVPWs declined from 1.09 mm to 0.68 mm (Figure 3b). In line with the cardiac dysfunction, the $Rnd3^{+/-}$ mice displayed higher mortality during the 3 weeks after TAC surgery compared with the WT control. The survival rates of these two genotype mice lines started to exhibit significant difference at the 7^{th} day post-TAC. And at the end-time point (21^{th} day), the survival rate of the mutant mice decreased to 75%, while the WT mice displayed a 93% survival rate (Figure 3c).

The Rnd3 deficient mice are predisposed to TAC induced hemodynamic stress, and developed heart failure with dilated cardiomyopathy phenotype, which suggests that Rnd3 plays an essential role in the transition of chronic heart failure.

Severe Cardiac Apoptosis was Detected in the $Rnd3^{+/-}$ Heart after TAC

It's well known that loss of cardiomyocytes results in heart dysfunction and dilated cardiomyopathy. To investigate the underlying mechanism of the $Rnd3^{+/-}$ heart failure development induced by TAC, I examined the hearts using histological and molecular analyses.

Figure 3. Rnd3$^{+/-}$ Mice Developed Dilated Cardiomyopathy Phenotype Induced by Pressure Overload. (a) Representative images from echocardiography indicate the enlarged left ventricle and thin left ventricular posterior wall in post-TAC Rnd3$^{+/-}$ mice. (b) Quantification of parameters LVIDs and LVPWs determined by echocardiography confirmed the dilated cardiomyopathy phenotype in Rnd3$^{+/-}$ heart induced by TAC. (c) Rnd3$^{+/-}$ mice exhibited a lower survival rate compared to the WT mice in 3 weeks after TAC. The number in each column represents animal numbers in each group. One-way ANOVA followed by Student-Newman-Keuls test was used for multiple group comparisons. The P value < 0.05 was considered as significant difference. Data are presented as means ± s.d. Scale bar represents 1mm. SP: septum; LVIDs: left ventricular internal dimension at systole; LVPWs: left ventricular posterior wall thickness at systole.

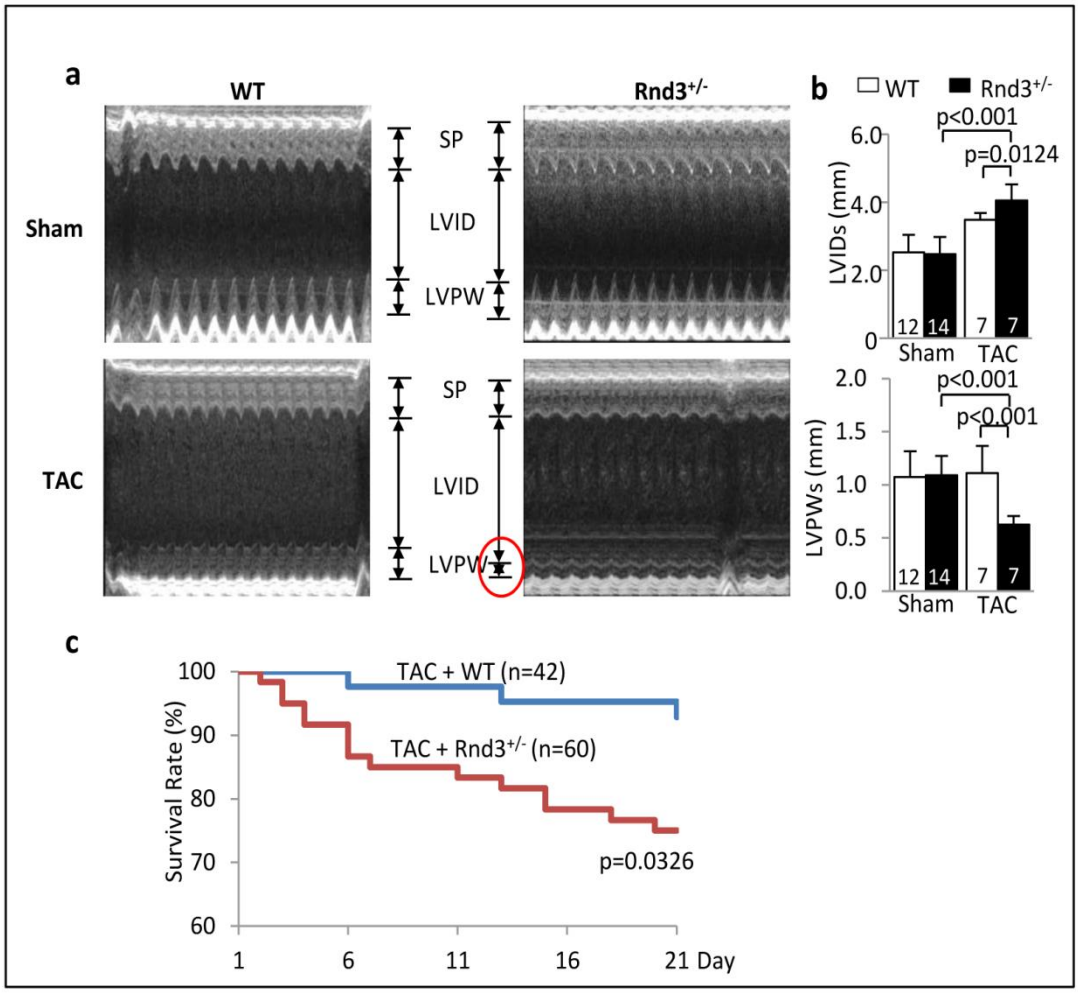

I harvested the hearts from the WT and Rnd3$^{+/-}$ mice before and after TAC, and analyzed the heart sections by terminal deoxynucleotidyl transferase dUTP nick end labeling (TUNEL), which is an immunochemical method to identify apoptotic cells. Cardiomyocytes were identified by F-actin immunochemical staining. Significant amount of apoptotic cardiomyocytes were observed in the mutant hearts compared with the WT hearts after TAC surgery (Figure 4a, b). Along with the histological analysis, the immunoblottings of caspase 3 were probed by antibody to detect the activation of caspase 3 in animal hearts. Increased active caspase 3 level was detected in the Rnd3$^{+/-}$ hearts after TAC, indicating the cardiac apoptosis development (Figure 4c, d).

Under hemodynamic stress the Rnd3$^{+/-}$ mice developed severe cardiac apoptosis, which suggested a potential mechanism in the Rnd3 deficiency mediated cardiomyopathy.

Figure 4. Rnd3$^{+/-}$ Mice Developed Cardiac Apoptosis in Response to TAC. (a) Representative images showed green fluoresce of terminal deoxynucleotidyl transferase dUTP nick end labeling (TUNEL) stained sections from WT and Rnd3$^{+/-}$ hearts after TAC. The images were overlapped with blue fluoresce of nuclei counter-staining. Cardiomyocytes were visualized by red fluoresce of F-actin Phalloidin staining. Arrows point at TUNEL positive cardiomyocytes. (b) Significant increases in TUNEL positive cardiomyocytes number were observed in Rnd3$^{+/-}$ hearts after TAC. Cell numbers were quantified by LAS V4.0 software. (c) Higher active caspase 3 levels were detected in Rnd3$^{+/-}$ hearts compared with WT control after TAC. (d) Densitometry quantification of active caspase 3 levels normalized by GAPDH. Casp3: Caspase 3; GAPDH: glyceraldehyde 3-phosphate dehydrogenase. The number in each column represents animal numbers in each group. One-way ANOVA followed by Student-Newman-Keuls test was used for multiple group comparisons. Unpaired, two-tailed student's t test was used for two group comparisons. The P value < 0.05 was considered as significant difference. Data are presented as means ± s.d. Scale bar represents 10μm.

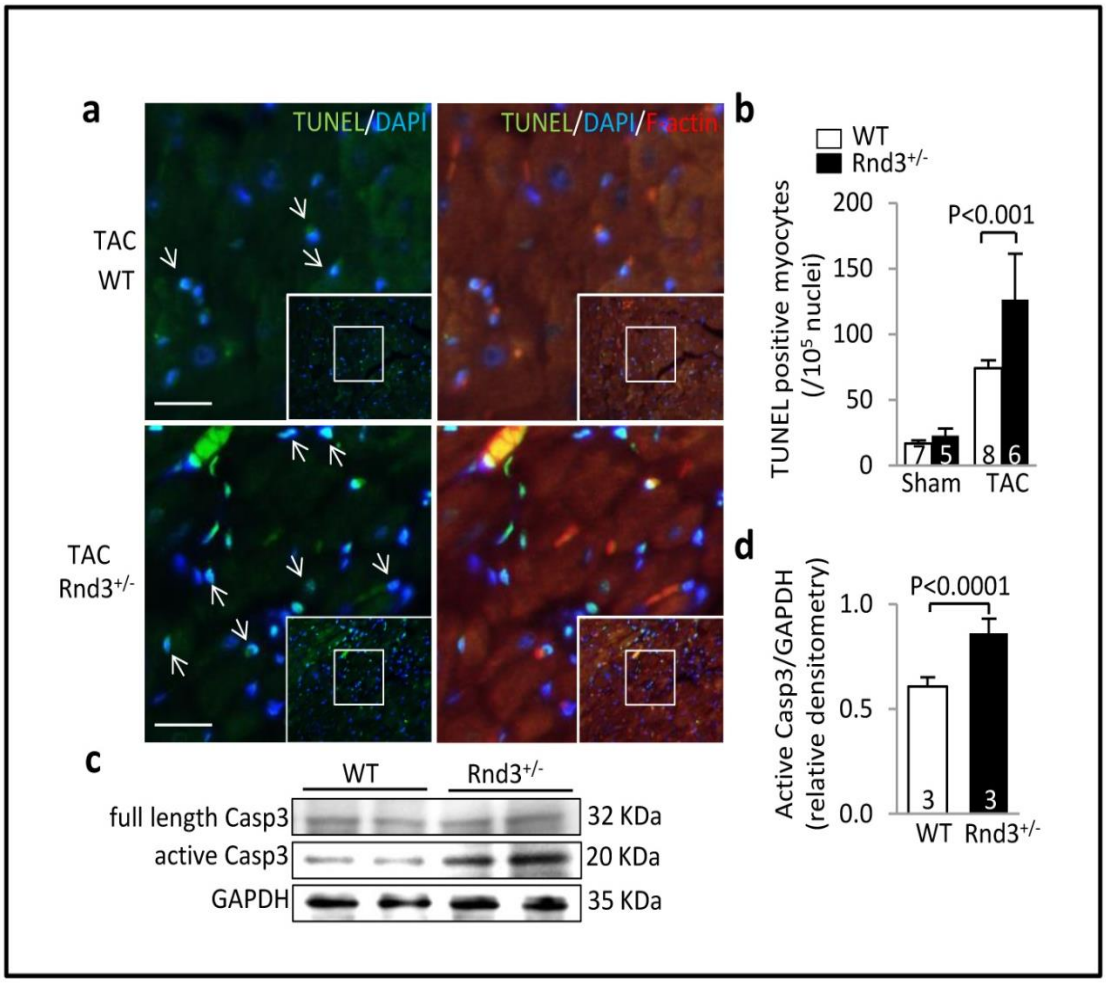

Complete Deletion of *Rnd3* Gene Spontaneously Resulted in Cardiac Apoptosis

The Rnd3-null mice were lethal appropriately at E11.0 stage with the heart failure developed at E10.5 stage. To investigate if loss of *Rnd3* gene would spontaneously result in cardiac apoptosis in physiological condition, the Rnd3-null embryonic hearts at E10.5 stage were adopted for histological analysis.

I collected $Rnd3^{-/-}$ hearts at E10.5 embryo stage and conducted TUNEL staining on the embryonic heart sections. Consistent with the apoptosis phenotype in the TAC stress remodeled adult $Rnd3^{+/-}$ heart, significant amount of apoptotic cardiomyocytes were also observed in the $Rnd3^{-/-}$ embryonic hearts under basal condition (Figure 5a, b). 40 pairs of WT and mutant embryonic hearts were collected for further immunoblotting analysis. The dramatically increased activity of apoptosis marker caspase 3 further confirmed the apoptosis phenotype in the Rnd3-null embryonic hearts (Figure 5c).

Along with the high lethality at embryo E11.0 stage, $Rnd3^{-/-}$ mice spontaneously developed heart failure and cardiac apoptosis at E10.5 stage. This result is consistent with the phenomenon in the post-TAC $Rnd3^{+/-}$ mice. Rnd3 deficiency is closely associated with the cardiac apoptosis, which is a novel discovery and probably can explain the meaning of Rnd3's down-regulation in the human failing hearts.

Figure 5. Severe Cardiac Apoptosis was Observed in the Rnd3$^{-/-}$ Embryonic Hearts at the E10.5 Stage. (a) Representative images showed green fluoresce of TUNEL stained WT and Rnd3$^{-/-}$ E10.5 embryonic cardiac sections. Cardiomyocytes were visualized by red fluoresce of F-actin Phalloidin staining. Arrows point at TUNEL positive cardiomyocytes. Scale bars represent 50μm and 20 μm, respectively. (b) Significant amounts of TUNEL positive cardiomyoctes were detected in Rnd3$^{-/-}$ embryonic hearts compared with WT controls. (c) Significant increased caspase 3 activities were detected in 40 Rnd3$^{-/-}$ embryonic hearts compared with 40 WT controls. Immunoblotting results were quantified by densitometry analysis. Casp3: Caspase 3; GAPDH: glyceraldehyde 3-phosphate dehydrogenase. The number in each column represents animal numbers in each group. Unpaired, two-tailed student's *t* test was used for two group comparisons. The P value < 0.05 was considered as significant difference. Data are presented as means ± s.d.

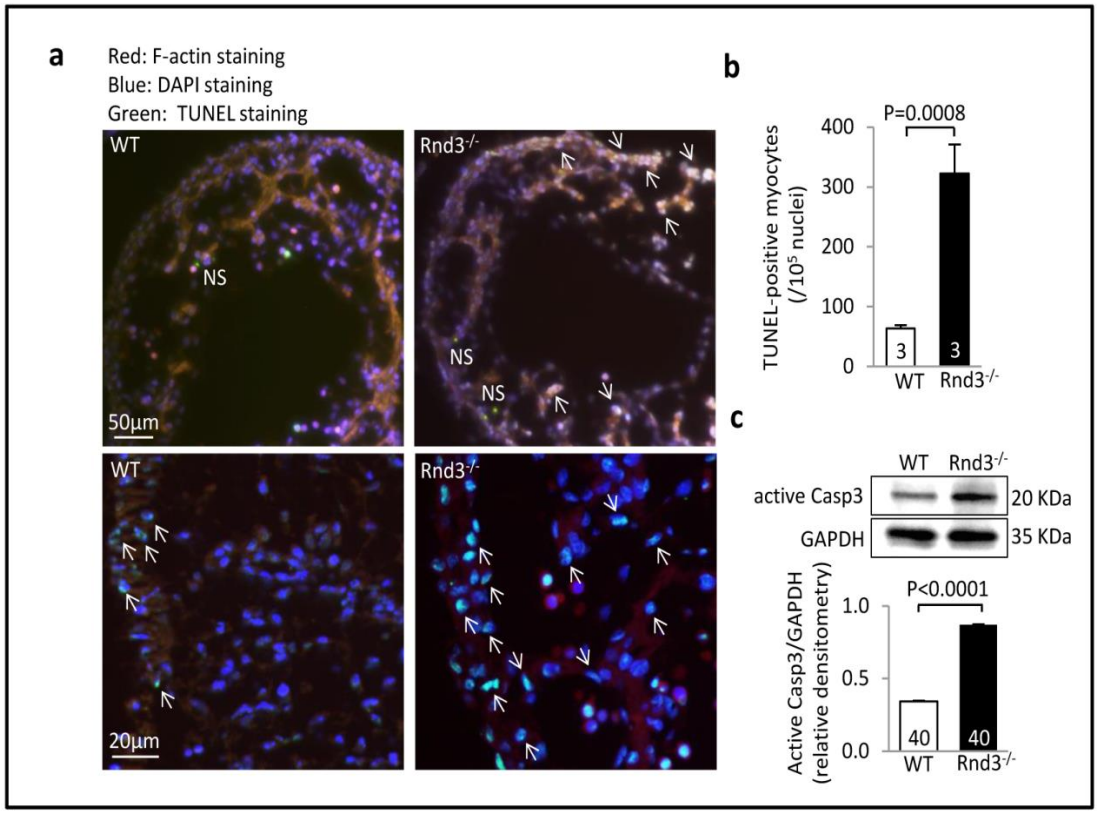

Rnd3 Deficiency Resulted in Cardiac Responsive Angiogenesis Defect

Responsive angiogenesis plays a vital role in cardiac repair after the exposure to ischemic stress. The heart needs microvessels to transport nutrients and oxygen. In chronic heart remodeling, both responsive angiogenesis and vasculogenesis are stimulated. This process is modulated by the co-work of chemokines, cytokines and growth factors. Compensatory angiogenesis disorder results in cardiac dysfunction, even heart failure. I analyzed microvasculature generation in the WT and the $Rnd3^{+/-}$ hearts and observed a second phenotype that Rnd3 deficiency resulted in cardiac responsive angiogenesis defect.

By labeling the endothelial cells with Isolectin-B4, the capillaries in cardiac tissue were visualized. The images were analyzed by LAS image analysis system, and the angiogenesis status was quantified based on the capillary areas and numbers. The WT and the $Rnd3^{+/-}$ hearts in sham group exhibited similar capillary number and area (Figure 6a, b, Sham). As I expected, the hemodynamic stress stimulated the angiogenesis compensation in the WT heart; however, in the mutant heart the responsive angiogenesis was failed. Smaller capillary areas and fewer capillary numbers were detected in the post-TAC $Rnd3^{+/-}$ heart compared to the WT control (Figure 6a, b, TAC).

Figure 6. Rnd3$^{+/-}$ Heart Developed Responsive Angiogenesis Defect under Hemodynamic Stress. (a) Isolectin-B4 stained cardiac capillaries (green) from WT and Rnd3$^{+/-}$ heart tissue sections before and after TAC. Nucleuses were visualized by blue DAPI staining. (b) Capillary area and number were quantified by LAS V4.0 software. Significant decreases in Rnd3$^{+/-}$ hearts were detected. The number in each column represents animal numbers in each group. One-way ANOVA followed by Student-Newman-Keuls test was used for multiple group comparisons. The p value < 0.05 was considered as significant difference. Data are presented as means ± s.d. Scale bar represents 25μm.

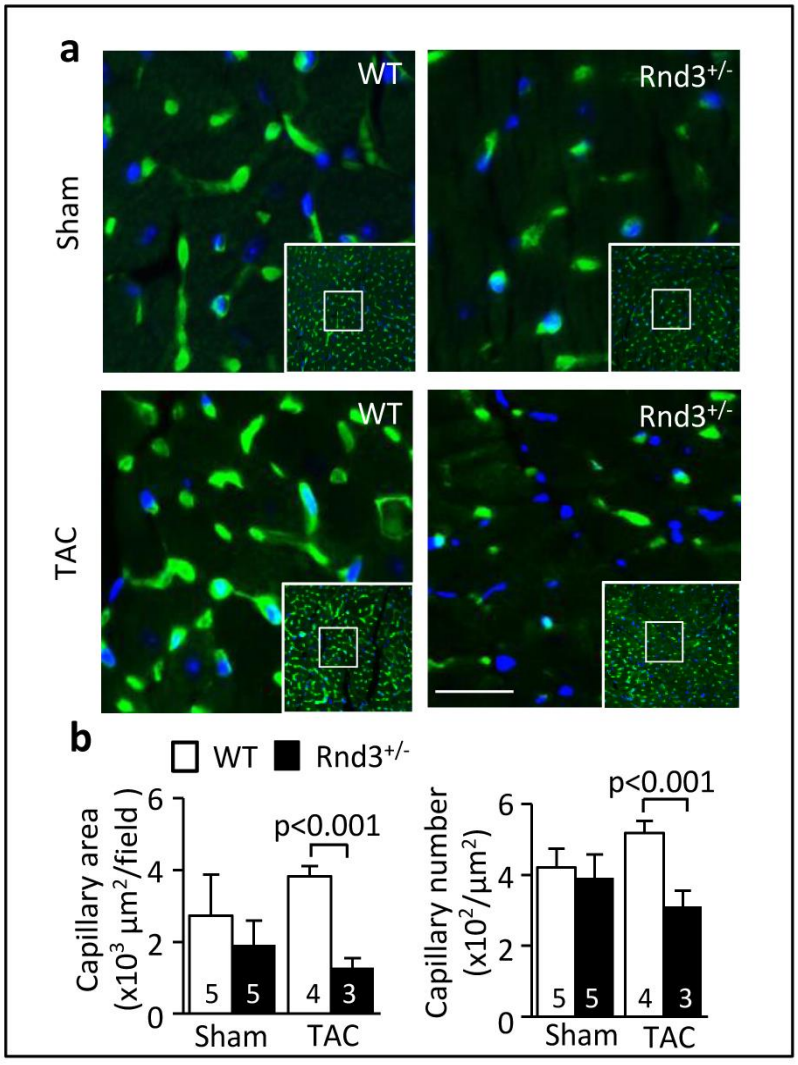

Coronary flow reserve (CFR) is a velocity index for blood flow through the capillaries derived from coronary artery. To estimate coronary capillary circulation, the CFR was assessed before and after TAC. The $Rnd3^{+/-}$ heart displayed similar microvessel function compared with the WT heart prior to TAC stress (Figure 7a, Sham). In response to stress, a 20.8% reduction of CFR was detected in the $Rnd3^{+/-}$ mice compared with the WT control, indicating the defective microvessel function in the Rnd3 mutant heart (Figure 7a, TAC).

The angiogenesis defect and ischemia induced hypoxia always serves as an indicator for testing angiogenesis deficiency *in vivo*. A chemical reagent, hypoxyprobe-1, can deposit to hypoxia region in live animal and can be visualized by immunohistochemical staining. Using this method, I observed a 5.9-fold increase in hypoxic area in the $Rnd3^{+/-}$ hearts compared with the WT control after TAC (Figure 7b, c).

Figure 7. Rnd3$^{+/-}$ Heart Developed Impaired Coronary Perfusion under Hemodynamic Stress. (a) Rnd3$^{+/-}$ mice displayed a reduction of coronary flow reserve after stress. (b) Hypoxic regions were labeled by Hypoxyprobe-1 staining (brown). Rnd3$^{+/-}$ cardiac tissue showed extensive hypoxia response compared with WT control after TAC. (c) Quantification of hypoxic area in WT and Rnd3$^{+/-}$ cardiac sections. A 5.9-fold increase was detected in Rnd3$^{+/-}$ hearts. The number in each column represents animal numbers in each group. One-way ANOVA followed by Student-Newman-Keuls test was used for multiple group comparisons. The p value < 0.05 was considered as significant difference. Data are presented as means ± s.d. Scale bar represents 25μm.

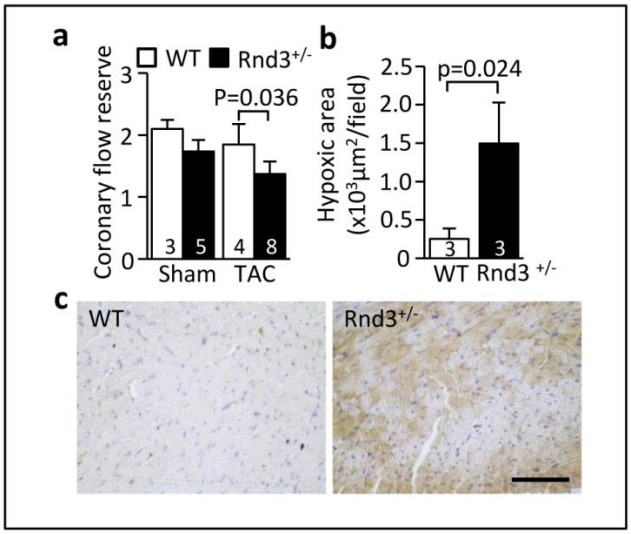

Evidenced by capillary histological analysis, circulation function assessment and hypoxic area measurement, the Rnd3$^{+/-}$ mice developed responsive angiogenesis disorder in heart under stress. Rnd3 deficiency mediated heart failure and dilated cardiomyopathy probably not only due to the increased cardiac apoptosis, but also due to the compromised compensatory ability to generate the functional new microvessels. Because of these two phenotypes, I will illustrate two different mechanisms to explain how Rnd3 takes part in the heart failure development.

Rho Kinase 1 Signaling Pathway was Activated by *Rnd3* Gene Deletion

Our lab's previous work has reported that Rho kinase 1 (ROCK1) is activated in human end-point failing hearts. And the activation has been implicated in cardiac apoptosis through manipulating the PTEN/Akt pathway mediated activation of caspase 3[42]. Therefore it's a logical thinking that Rnd3, the endogenous inhibitor of ROCK1, probably also plays a regulatory role in apoptosis, contributing to the dilated cardiomyopathy *in vivo*.

The activity of ROCK1 in the mouse hearts was detected by immunoblotting. Myosin phosphatase target subunit 1 (MYPT1) and myosin light chain 2 (MLC2) served as the substrates of ROCK1. The phosphorylation status of these substrates indicated the activity of ROCK1. Hyper-phosphorylated MYPT1 was observed in the $Rnd3^{+/-}$ hearts after TAC, indicative of the elevated ROCK1 activity (Figure 8a, b). Meanwhile, I also detected ROCK1 pathway in $Rnd3^{-/-}$ hearts at embryo E10.5 stage. Again, the ROCK1 pathway was significantly activated by complete deletion of Rnd3, determined by the hyper-phosphorylated MYPT1 and MLC2 (Figure 8c, d).

Associated with the heart failure and apoptotic phenotype, the elevation of ROCK1 signaling pathway was detected in the $Rnd3^{-/-}$ embryo hearts under physiological condition and in the $Rnd3^{+/-}$ hearts under pathological condition. These data suggested that the Rnd3 deficiency mediated cardiac apoptosis probably due to the activation of ROCK1.

Figure 8. Activation of ROCK1 Signaling Pathway was Observed in the Rnd3$^{+/-}$ Heart Post-TAC as Well as in the Rnd3$^{-/-}$ Embryonic Heart. (a) Elevated ROCK1 activities were observed in Rnd3$^{+/-}$ hearts compared with WT hearts after TAC, determined by the increased ROCK1 substrate MYPT1 phosphorylation level. (b) Densitometry quantification of p-MYPT1 levels normalized by total MYPT1. (c) Increased phosphorylation levels of ROCK1 substrate MYPT1 and MLC2 demonstrated elevated ROCK1 activities in Rnd3-null hearts. (d) Densitometry quantifications of p-MYPT1 levels normalized by total MYPT1, and p-MLC2 levels normalized by total MLC2. ROCK1: Rho kinase 1; MYPT1: myosin phosphatase target subunit 1; MLC2: myosin light chain 2. The number in each column represents animal numbers in each group. Unpaired, two-tailed student's t test was used for two group comparisons. The P value < 0.05 was considered as significant difference. Data are presented as means ± s.d.

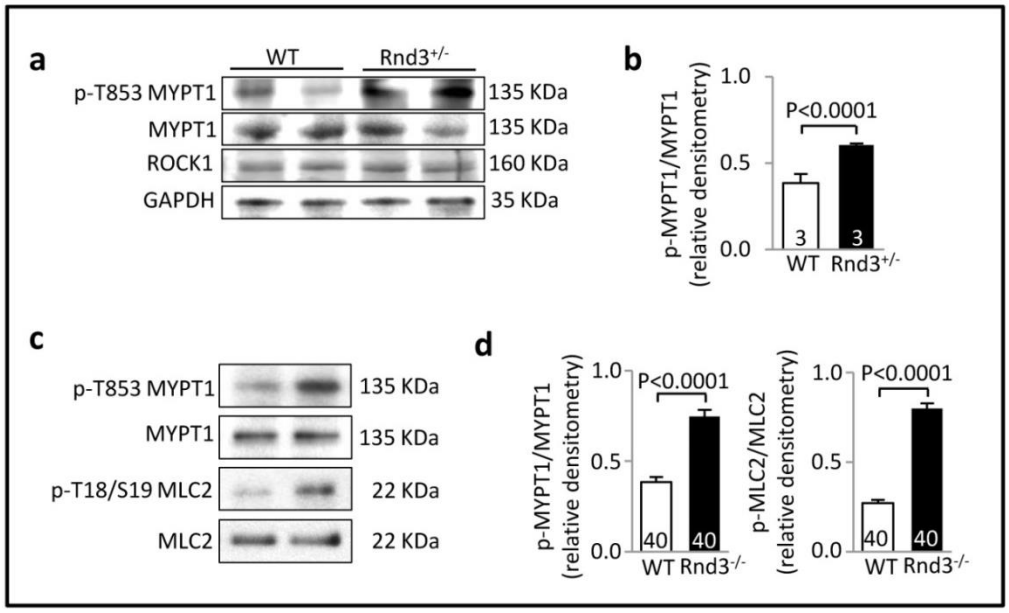

Rho Kinase Inhibitor, Fasudil Partially Rescued Heart Failure and Cardiac Apoptosis in the Rnd3$^{+/-}$ Heart after TAC

The Rnd3$^{+/-}$ mice were predisposed to hemodynamic stress and developed cardiac apoptosis, which is consistent with the phenotype in Rnd3 null mice at embryonic stage.

More evidences showed that the activated ROCK1 pathway was closely associated with the apoptosis in Rnd3 deficient hearts. Since Rnd3 can physically bind to and suppress ROCK1 activity, I hypothesized that Rnd3 deficiency mediated cardiac apoptosis probably through the ROCK1 activation. To verify this hypothesis, I conducted a rescue experiment by the application of Fasudil, a clinical used ROCK1 inhibitor.

Mice were exposed to the hemodynamic stress and the Fasudil was administrated immediately after TAC surgery. Treatment and TAC stress were lasted for three weeks. Echocardiographs were recorded for the assessments of cardiac function and morphological remodeling. Cardiac functions in the post-TAC $Rnd3^{+/-}$ mice were significantly improved by Fasudil compared with the non-treated mice. The increases in ejection fraction (EF) and fractional shortening (FS) were observed from 19.1% and 8.6% to 40.3% and 19.5%, respectively (Figure 9a). However, these improvements did not make the heart function been fully rescued. The pressure overloading stimulated myocardium apoptosis in the $Rnd3^{+/-}$ heart was attenuated by the Fasudil treatment (Figure 9b). The apoptotic cardiomyocyte number was reduced by 63.5% after the treatment (Figure 9c). Along with the decrease in apoptotic cell number, the up-regulation of active caspase 3 protein level in the post-TAC $Rnd3^{+/-}$ heart was significantly eased by Fasudil (Figure 9d, e). Western blotting of the phosphorylated ROCK1 substrate, MYPT1, demonstrated that ROCK1 signaling was repressed by the Fasudil (Figure 9f, g).

Figure 9. Rnd3 Deficiency Mediated Apoptotic Cardiomyopathy and Heart Failure were Partially Rescued by ROCK1 Inhibitor Fasudil. (a) Cardiac functions for sham, TAC and TAC plus Fasudil groups measured by echocardiography. (b) Representative images showed green fluoresce of TUNEL stained Rnd3$^{+/-}$cardiac sections from sham, TAC and TAC plus Fasudil groups. The images were overlapped with blue fluoresce of nuclei counter-staining. Cardiomyocytes were visualized by red fluoresce of F-actin Phalloidin staining. Arrows point at TUNEL positive cardiomyocytes. (c) Less TUNEL positive cardiomyocytes were observed in Fasudil treated Rnd3$^{+/-}$ mice heart after TAC. (d) Immunoblotting of apoptosis marker full-length Casp3 and active Casp3 in Rnd3$^{+/-}$ mice heart before and after TAC, with and without Fasudil treatment. (e) Densitometry analysis for active Casp3 level normalized by GAPDH. (f) Immunoblotting of ROCK1 substrate p-T853 MYPT1 and total MYPT1 in Rnd3$^{+/-}$ mice heart before and after TAC, with and without Fasudil treatment. (g) Densitometry analysis for p-MYPT1 level normalized by total MYPT1. The number in each column represents animal numbers in each group. One-way ANOVA followed by Student-Newman-Keuls test was used for multiple group comparisons. The P value < 0.05 was considered as significant difference. Data are presented as means ± s.d. Scale bar represents 10μm.

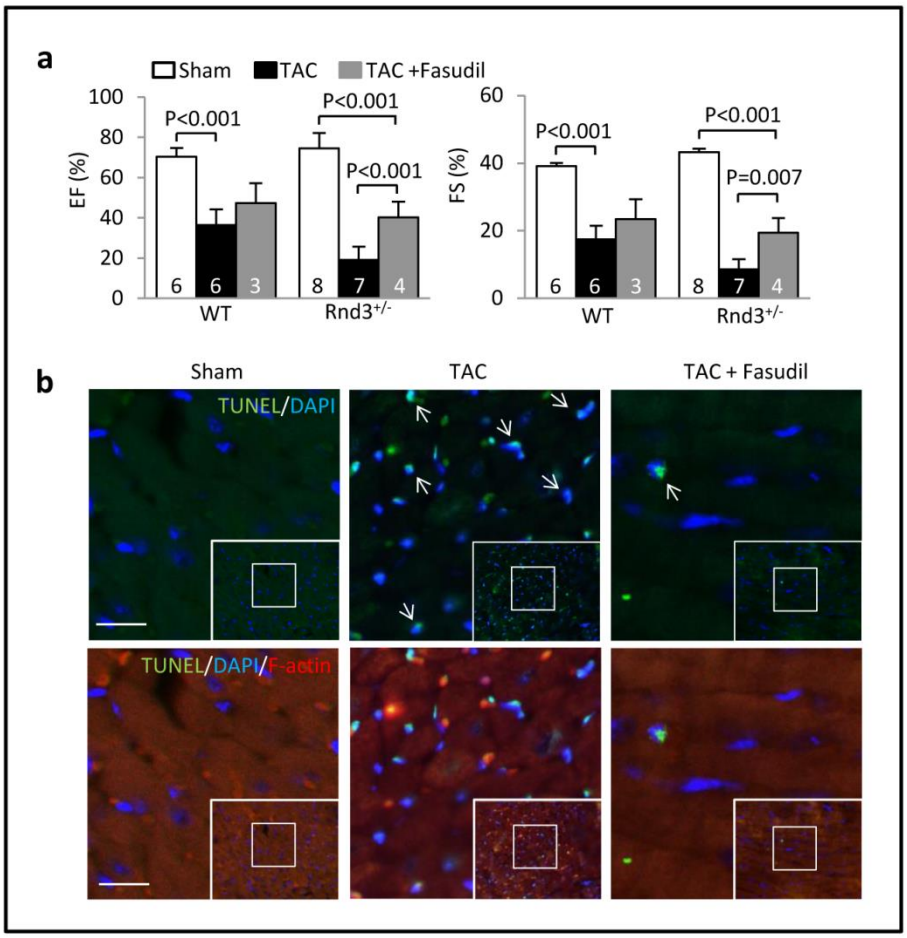

Figure 9. Continued.

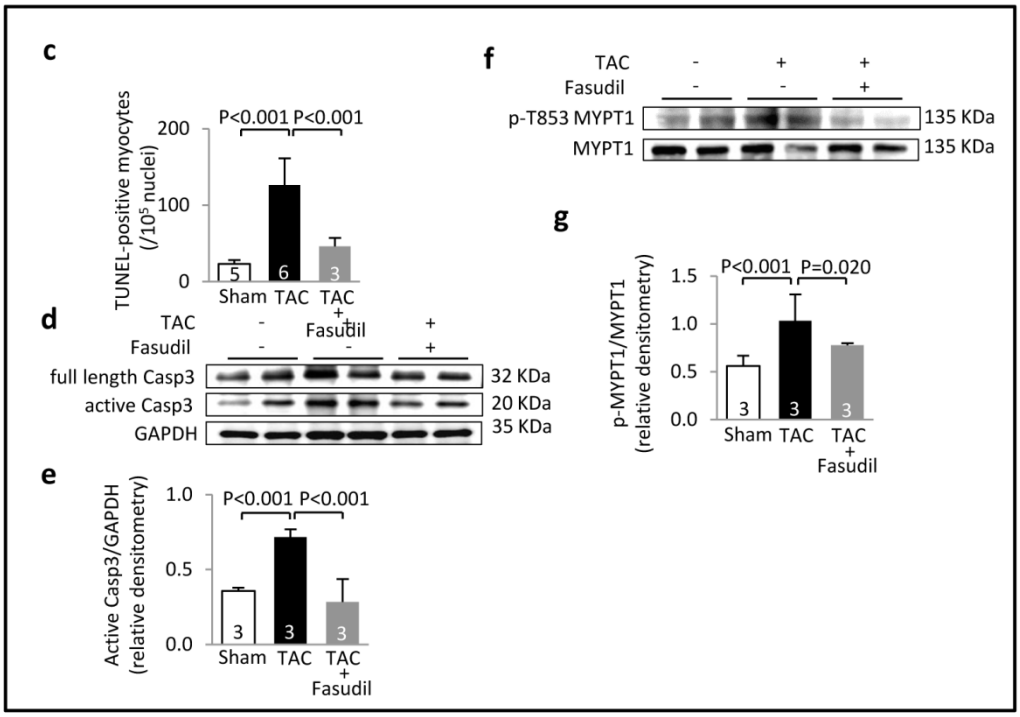

Given that ROCK1 modulates smooth muscle contractility through regulating actin assembly, ROCK1 plays a critical role in control of vessel tone and blood pressure. Fasudil is a selective Rho kinases inhibitor and vasodilator. To delineate whether the improved cardiac phenotype was not due to Fasudil mediated vasodilation, I assessed both systolic blood pressure and diastolic blood pressure for the WT mice and $Rnd3^{+/-}$ mice before and after TAC, with or without Fasudil treatment. The $Rnd3^{+/-}$ mice exhibited no significant blood pressure changes among these multiple groups compared with the WT mice (Figure 10).

In this rescue experiment, blockage of ROCK1 pathway significantly ameliorated heart failure and apoptosis in Rnd3 mutant heart after surgery. Therefore, the Rnd3 deficiency mediated apoptotic cardiomyopathy is partially regulated by the ROCK1 signaling pathway activation.

Figure 10. Blood Pressures of the WT and the Rnd3+/- Mice were Not Changed after Fasudil Treatment. (a) Systolic blood pressure was assessed in the WT and the Rnd3$^{+/-}$ mice among multiple groups. (b) Diastolic blood pressure was calculated based on the systolic blood pressure. The number in each column represents animal numbers in each group. Kruskal-Wallis One Way ANOVA on Ranks followed by Dunn's method was used for multiple group comparisons. The P value < 0.05 was considered as significant difference. Data are presented as means ± s.d.

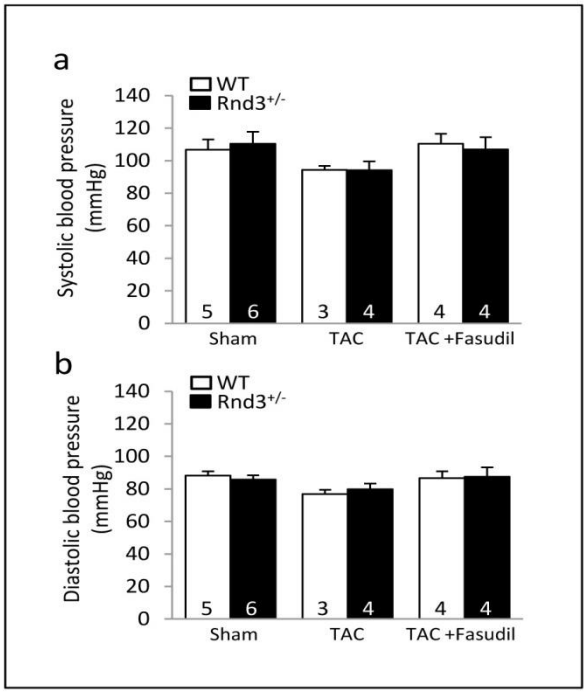

Genetic Deletion of ROCK1 Attenuated Rnd3 Deficiency Mediated Apoptotic Cardiomyopathy

The Fasudil *in vivo* rescue experiment indicated that cardiac apoptosis in Rnd3 knockout mice may partially due to the activation of ROCK1 signaling. However, the potential side-effect and non-specificity of the Fasudil weakened the conclusion. To further demonstrate that the ROCK1 activation mechanism was responsible for the Rnd3 deficiency-mediated cardiomyopathy, a second animal rescue experiment was performed. Genetic deletion of *ROCK1* was the other strategy to verify the ROCK1 pathway in Rnd3 defective mice.

I generated a double-knockout (DKO) mouse line with the genotype of $Rnd3^{+/-/ROCK1-/-}$ (Figure 11a). The DKO mice exhibited normal cardiac function under physiological condition (Figure 11b, Sham). Then, both of the $Rnd3^{+/-}$ mice and $Rnd3^{+/-/ROCK1-/-}$ mice were exposed to the TAC surgery induced cardiac pressure overload. Echocardiography was recorded 3 weeks post the surgery. Consistent with the previous studies, the $Rnd3^{+/-}$ mice developed heart failure. However, the post-TAC cardiac function in $Rnd3^{+/-/ROCK1-/-}$ mice (EF 52.9% and FS 26.5%) was much better than $Rnd3^{+/-}$ mice (EF 19.9% and FS 8.9%) (Figure 11b, TAC). Cardiac apoptosis was compared in both two mouse lines. Less TUNEL positive cardiomycytes numbers as well as lower active casepase 3 level were observed in the DKO mice compared with the $Rnd3^{+/-}$ mice (Figure 11c to f).

Figure 11. Genetic Deletion of *ROCK1* Partially Improved Cardiac Function and Attenuated Apoptosis in the Post-TAC Rnd3$^{+/-}$ Mice. (a) Genotyping profile showed the establishment of the double-knockout (DK) mouse line, Rnd3$^{+/-ROCK1-/-}$. (b) Cardiac functions of Rnd3$^{+/-}$ mice and DK mice before and after TAC. (c) Representative images for TUNEL staining in cardiac sections from Rnd3$^{+/-}$ mice and DK mice after TAC (green). Arrows point at TUNEL positive cells overlapped with nuclei counter-staining (blue). Cardiomyocytes were visualized by Phalloidin staining for F-actin (red). (d) Less TUNEL positive cardiomyocytes were observed in DK mice compared with Rnd3$^{+/-}$ mice. (e) Immunoblotting of apoptosis marker full-length Casp3 and active Casp3 in Rnd3$^{+/-}$ and DK mouse hearts before and after TAC. (f) Densitometry analysis for active Casp3 level normalized by GAPDH. The number in each column represents animal numbers in each group. One-way ANOVA followed by Student-Newman-Keuls test was used for multiple group comparisons. The P value < 0.05 was considered as significant difference. Data are presented as means ± s.d. Scale bar represents 10μm.

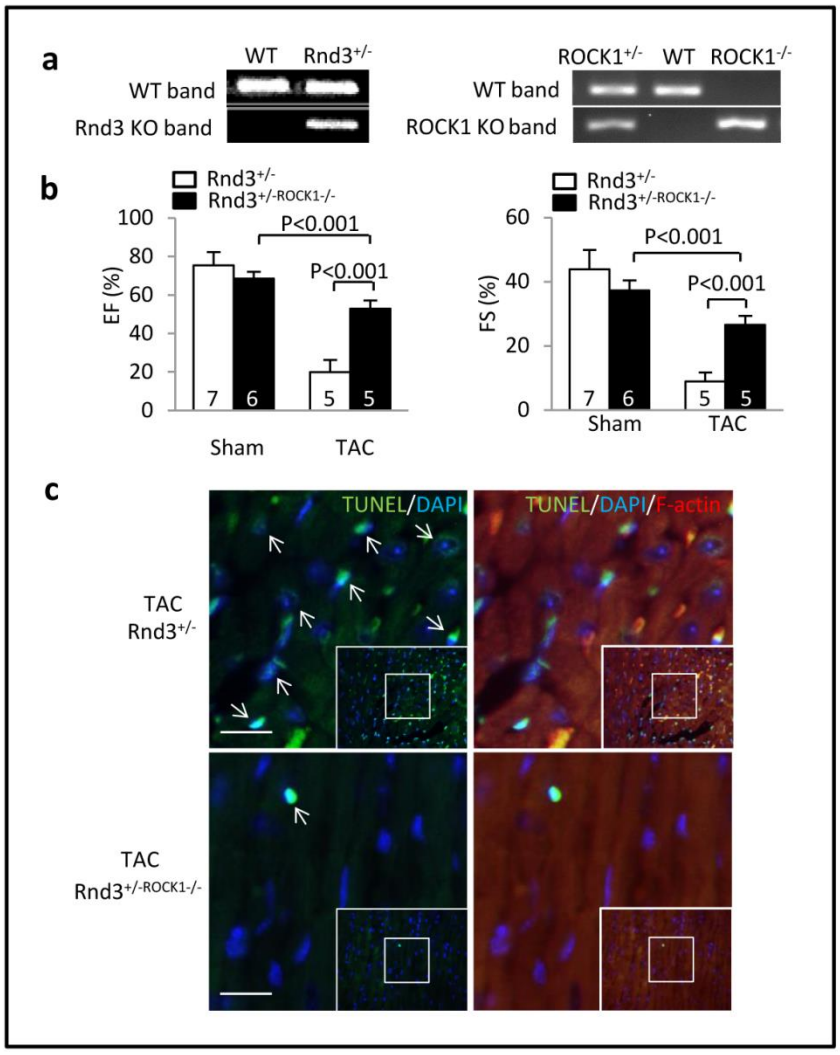

Figure 11. Continued

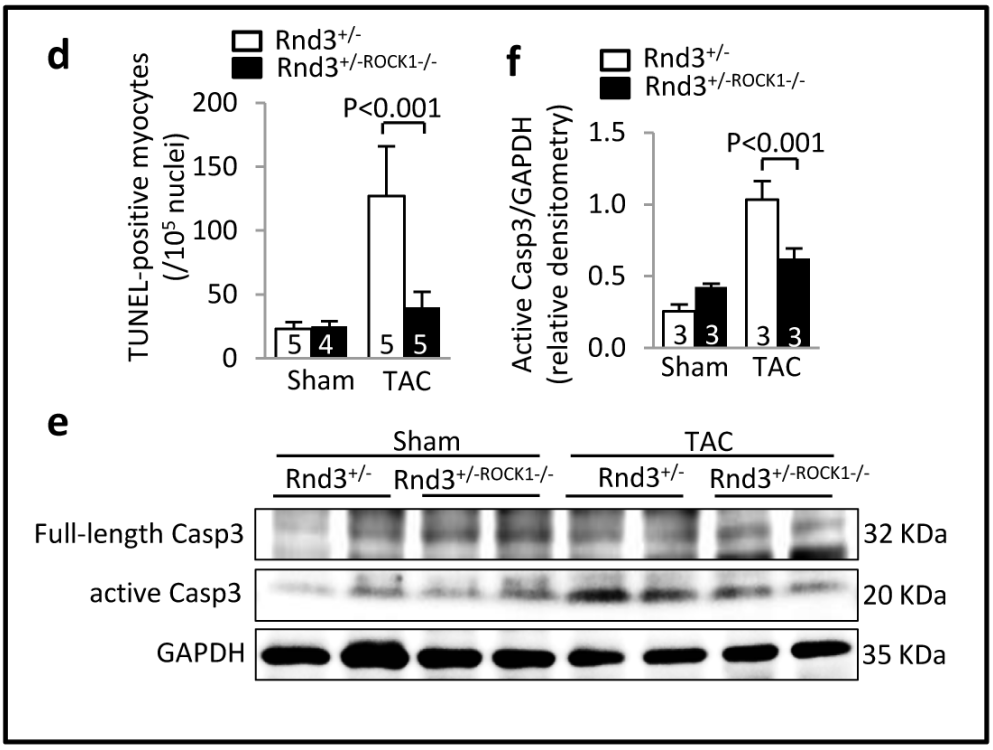

Genetic deletion of *ROCK1* significantly, however not completely, rescued the impaired heart function and apoptosis caused by the Rnd3 deficiency. These data suggested that ROCK1 only partially contributed to the Rnd3 mediated cardiac apoptosis. The ROCK1 independent mechanism is interesting and worthy to be investigated. Furthermore, in the $Rnd3^{+/-}$ mice heart failure model, the responsive angiogenesis defect could be another factor contributing to the cardiac dysfunction. Therefore my next study was focused on its underlying mechanism.

Key Pro-angiogenic Factors, HIF1α and VEGFA were Down-regulated in the Rnd3$^{+/-}$ Heart in Response to Pressure Overload

Besides the cardiac apoptosis, the responsive angiogenesis is another vital factor in the chronic heart remodeling and the heart failure development. Hypoxia-inducible factor 1 (HIF1)-vascular endothelial growth factor A (VEGFA) is one of the most important pathways promoting angiogenesis. In heart, cardiomyocyte is the major resource of VEGFA. VEGFA directly promotes endothelial cell proliferation, migration and increases vascular permeability in the angiogenesis process. The regulation of VEGFA is majorly at the transcriptional level by the transcription factors HIF1 and peroxisome proliferator-activated receptor-gamma coactivator (PGC)-1α. In order to investigate the mechanism underlying the responsive angiogenesis defect in the post-TAC Rnd3$^{+/-}$ heart, the expression levels of these angiogenic factors in heart were detected.

The HIF1-VEGFA signaling pathway was detected in the WT and Rnd3$^{+/-}$ hearts. The VEGFA protein level as well as the mRNA level was significant decreased in the Rnd3$^{+/-}$ heart after TAC compared with the WT control (Figure 12a, b). Along with the decreased VEGFA expression, HIF1α, the regulator of VEGFA, was also found down-regulated in Rnd3$^{+/-}$ heart (Figure 12a). To investigate the effect of Rnd3 on the crosstalk between the cardiomyocyte and the endothelium, a tube formation assay was performed. The primary WT and Rnd3$^{+/-}$ cardiomyocytes were isolated from post-TAC hearts, and then the conditional medium was applied on the human umbilical vein endothelial cells (HUVECs) to induce tube formation. After 6 hours the HUVECs developed mature tube

structure in the conditional medium. In the conditional medium from $Rnd3^{+/-}$ cardiomyocytes, the HUVECs displayed lower angiogenesis ability compared with the WT group, with the less branching points and less loop formations (Figure 12c, d). This experiment indicated that compared with the WT conditional medium, the $Rnd3^{+/-}$ conditional medium contained low level angiogenic factors. In order to dissect out which angiogenic factor plays more important role in this HUVECs tube formation assay, I detected the conditional medium, and found that the $Rnd3^{+/-}$ cardiomyocytes released less VEGFA into the medium compared with the WT control (Figure 12e).

Figure 12. HIF1-VEGFA Axis was Down-Regulated in the Rnd3$^{+/-}$ Heart after TAC. (a) Down-regulation of VEGFA and HIF1α protein levels were observed in Rnd3$^{+/-}$ heart tissue. (b) mRNA levels of VEGFA in WT and Rnd3$^{+/-}$ hearts were detected with or without TAC surgery stress. Significant decrease was observed in Rnd3$^{+/-}$ hearts. (c) Representative images of HUVECs tube formation assay induced by the conditional media from WT and Rnd3$^{+/-}$ cardiomyocytes. Fewer tubes were formed in the media from Rnd3$^{+/-}$ cardiomyocytes compared with WT control. Scale bar represents 200μm. (d) Quantification of HUVECs tube formation analyzed by Wimtube software. Fewer branching points and loops were detected in Rnd3$^{+/-}$ group. (e) Decreased secretion of VEGFA from Rnd3$^{+/-}$ cardiomyocytes into media was detected. The number in each column represents animal numbers in each group. One-way ANOVA followed by Student-Newman-Keuls test was used for multiple group comparisons. The p value < 0.05 was considered as significant difference. Data are presented as means ± s.d.

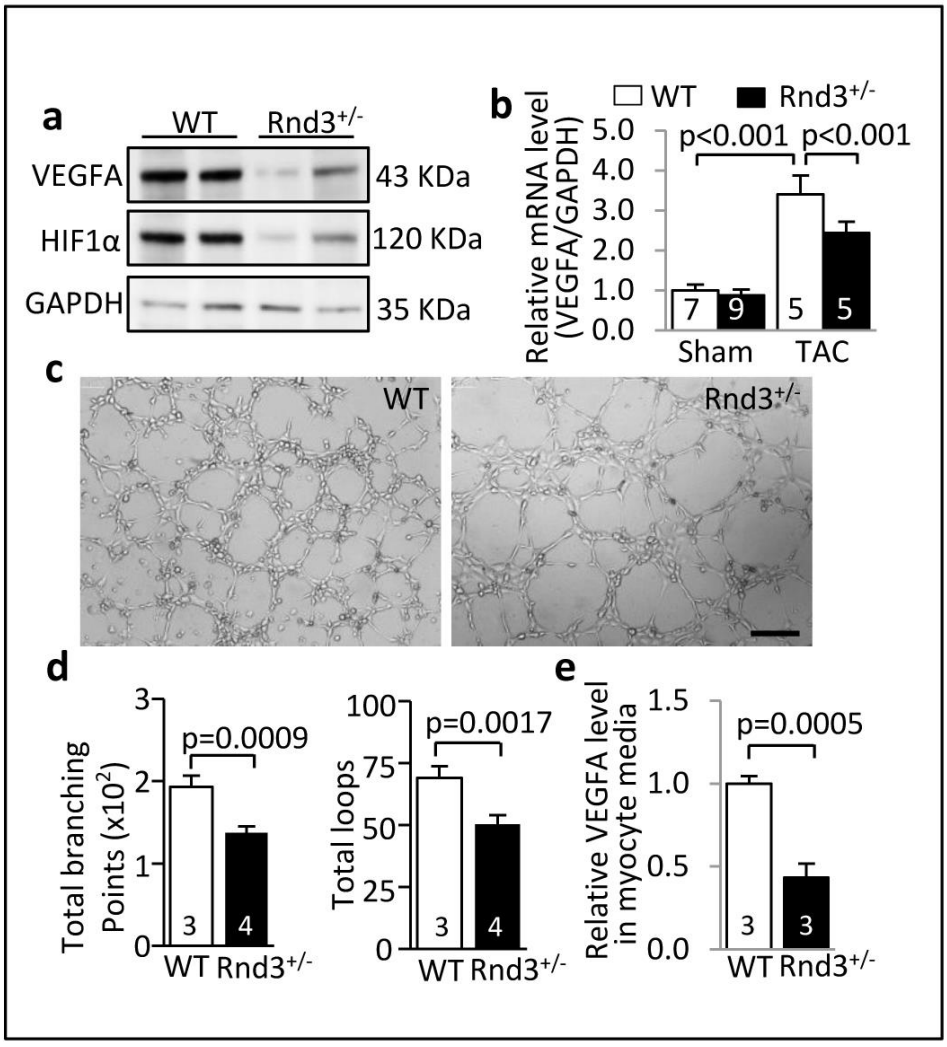

The reduction of VEGFA expression in Rnd3$^{+/-}$ heart tissue after surgery is consistent with the failed responsive angiogenesis in Rnd3$^{+/-}$ heart. As the major source of VEGFA, the cardiomyocyte affects the proliferation and migration of the endothelial cell in a paracrine manner. In response to stress stimulus, Rnd3 deficiency resulted in a decline of VEGFA produced from the cardiomyocyte, consequently leaded to the angiogenesis defect in heart. HIF1α, the major regulator of VEGFA, was found down-regulated in Rnd3$^{+/-}$ heart suggesting a potential mechanism that Rnd3 regulated angiogenesis by modulating HIF1α pathway.

Rnd3 Stabilized HIF1α through Physical Interaction

The regulation of HIF1α depends on oxygen sensitive post-translational modification. Under normoxia condition, HIF1α is hydroxylated by the enzyme prolyl hydroxylases (PHDs) and subsequently degraded by the ubiquitin-proteasome system (UPS). While under hypoxia condition, the activity of PHDs is blocked resulting in the stabilization of HIF1α. The accumulated HIF1α translocates into the nucleus and initiates the transcriptions of downstream target genes. To explore the mechanism underlying the down-regulation of the HIF1α-VEGFA pathway in Rnd3$^{+/-}$ heart, I performed a series of gain-loss function experiments manipulating the Rnd3 expression in Hela cell line.

HIF1α protein disappeared when Rnd3 was knocked down (Figure 13a), and accumulated gradually along with the Rnd3 overexpression in a dose-dependent manner (Figure 13b). When cells overexpressed Rnd3, the accumulation of endogenous HIF1α in nuclei was observed by immunostaining (Figure 13c). Consistent with the changes in

HIF1α protein levels, the expression of VEGFA was changed in the same pattern (Figure 13a, b). To further investigate the potential mechanism of Rnd3 induced HIF1α protein stabilization, I conducted an *in vitro* GST-Rnd3 pull-down experiment with the lysate from the cells overexpressing HA-HIF1α. The physical binding of GST-Rnd3 with HA-HIF1α was detected (Figure 13d). A further mutual co-immunoprecipitation assay was performed with the lysate from the cells transiently overexpressing Myc-Rnd3 and HA-HIF1α, the two proteins physically interacting with each other *in vivo* was observed (Figure 13e). Given that HIF1α functions as a transcription factor, I performed a luciferase assay to study whether Rnd3 regulated HIF1α transcriptional activity. A VEGFA promoter containing three repeats of HIF1 response elements (HRE) was cloned into luciferase reporter. Hypoxia treatment was applied to trigger HIF1α expression. Initiated by hypoxia condition, Rnd3 knock-down resulted in a 47% reduction in the HIF1α transcriptional activity compared with the WT control (Figure 13f). Consistent with the decreased HIF1α activity in Rnd3 deficient cell, VEGFA mRNA level decreased responsively (Figure 13g). Taken together, Rnd3 directly bound to and facilitated the HIF1α protein accumulation. Rnd3 deficiency weakened the transcription activity of HIF1α and the expression of its downstream target genes VEGFA.

Figure 13. Rnd3 Physically Interacted with HIF1α and Facilitated Its Stability. (a) Significant decreases in HIF1α and VEGFA protein levels were detected in cells knocked down Rnd3. (b) The protein levels of HIF1α and VEGFA gradually increased along with Rnd3 over expression in cells. (c) Representative images displayed that HIF1α accumulated in nuclei when cells overexpressing Rnd3. Scale bar represents 50μm. (d) HA-HIF1α was pull-downed by GST-Rnd3 *in vitro*. (e) Myc-Rnd3 and HA-HIF1α physically interacted in the *in vivo* mutual co-immunoprecipitation experiments. (f) Rnd3 knock-down restrained the HIF1α transcription activity evidenced by luciferase assay. (g) The Q-PCR result showed that Rnd3 deficiency resulted in VEGFA losing response to hypoxia. Unpaired, two-tailed student's *t* test was used for two group comparisons. The p value < 0.05 was considered as significant difference. Data are presented as means ± s.d.

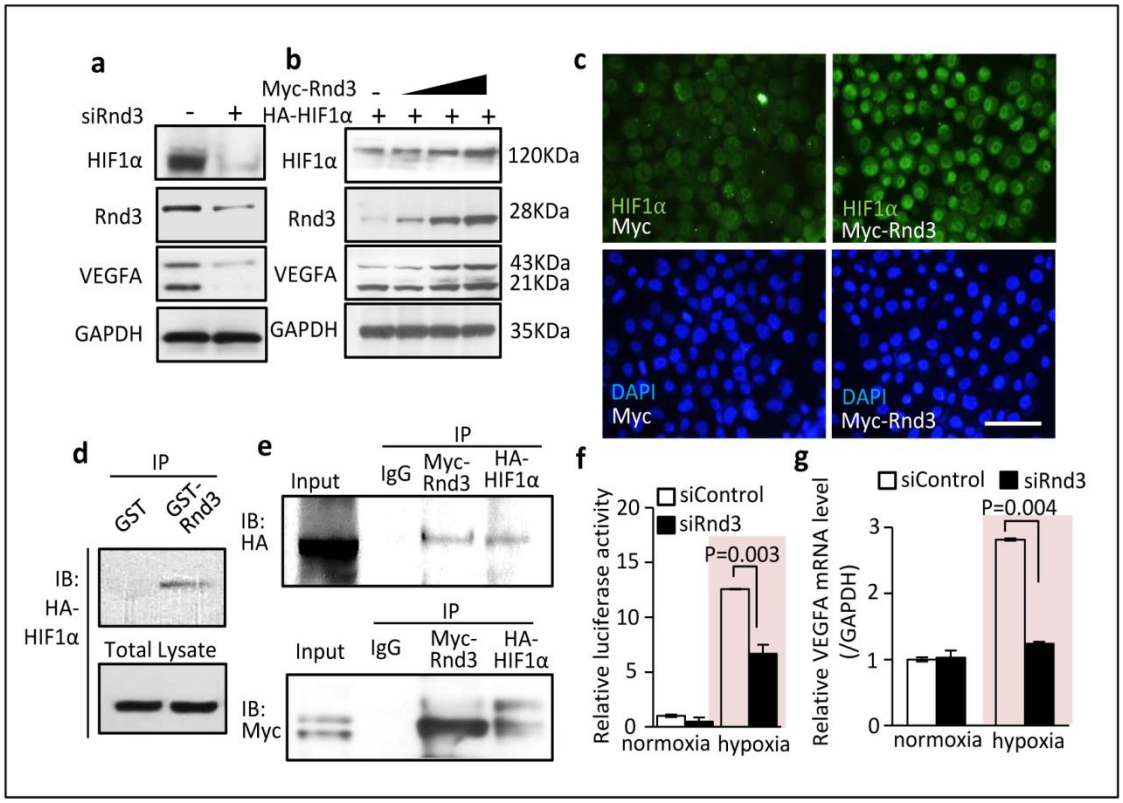

Cobalt Chloride, a HIF1α Stabilizer, Partially Attenuated Rnd3 Deficiency Mediated Dilated Cardiomyopathy

Given that the HIF1α-VEGFA pathway was suppressed in the $Rnd3^{+/-}$ heart, and that Rnd3 stabilized HIF1α and regulated its transcriptional activity in Hela cells, I hypothesized that the responsive angiogenesis defect in $Rnd3^{+/-}$ heart was probably due to Rnd3 deficiency induced HIF1α hyper-degradation. To test this hypothesis, I applied a HIF1α stabilizer on the $Rnd3^{+/-}$ mice and measured its effects on cardiac function and remodeling after TAC.

Cobalt chloride ($CoCl_2$) acts as an inhibitor of prolyl hydroxylases (PHDs), which hydroxylates HIF1α and consequently results in the degradation of HIF1α. The application of $CoCl_2$ stabilizes HIF1α protein and leads to its accumulation. WT and $Rnd3^{+/-}$ mice were exposed to TAC stress with $CoCl_2$ treatments for 3 weeks. After the administration of $CoCl_2$, significant improved heart function was observed in $Rnd3^{+/-}$ mice after TAC, with a 61% increase in ejection fraction (EF) and a 68% increase in fraction shortening (FS) (Figure 14a). The dilated left ventricle chamber and thin ventricular wall caused by TAC stress in $Rnd3^{+/-}$ heart were ameliorated by $CoCl_2$, evidenced by H&E staining (Figure 14b) and echocardiography analysis (Figure 14d). In post-TAC $Rnd3^{+/-}$ mice, the average ratio of lung weight (LW) over body weight (BW) decreased from 19.6 (none-treatment group) to 7.9 (treatment group), and the average ratio of LW over tibia length (TL) decreased from 24.8 (none-treatment group) to 13.3

(treatment group) (Figure 14c), demonstrating the rescued lung edema which were caused by severe heart failure.

To summarize the rescue experiments on $Rnd3^{+/-}$ mouse model, $CoCl_2$ significantly improved cardiac function and attenuated heart dilation by stabilizing HIF function, which suggested that Rnd3 deficiency mediated dilated cardiomyopathy partially through HIF1α destabilization.

Cobalt Chloride Improved Responsive Angiogenesis in the $Rnd3^{+/-}$ Hearts by Stabilizing HIF1α

My data indicated that the $CoCl_2$ mediated HIF1α stabilization played a critical role in the transition of $Rnd3^{+/-}$ heart to failure. I still have a question that whether the preserved $Rnd3^{+/-}$ heart function benefits from the angiogenesis promoted by HIF1α accumulation? To address this question, I checked the HIF1α-VEGFA pathway and the mouse cardiac capillary perfusion.

Figure 14. Cobalt Chloride Partially Ameliorated Rnd3 Deficiency Mediated Dilated Cardiomyopathy. (a) Cardiac function impairment in $Rnd3^{+/-}$ mice induced by TAC was partially attenuated after $CoCl_2$ treatment. (b) H&E staining of cardiac sections from WT and $Rnd3^{+/-}$ mice after TAC, with and without $CoCl_2$ treatment. Scale bar represents 1mm. (c) The ratio of lung weight over body weight and lung weight over tibia length indicated that $CoCl_2$ prevented heart failure development in $Rnd3^{+/-}$ mice after TAC. (d) The LVPWs and LVIDs of the hearts from WT and $Rnd3^{+/-}$ mice with or without $CoCl_2$ treatment before and after TAC were compared among groups. TAC stress induced dilated cardiomyopathy in $Rnd3^{+/-}$ heart was partially rescued by $CoCl_2$. LVPWs: and left ventricular posterior wall thickness at systole; LVIDs: left ventricular internal dimension at systole. The number in each column represents animal numbers in each group. One-way ANOVA followed by Student-Newman-Keuls test was used for multiple group comparisons. The p value < 0.05 was considered as significant difference. Data are presented as means ± s.d.

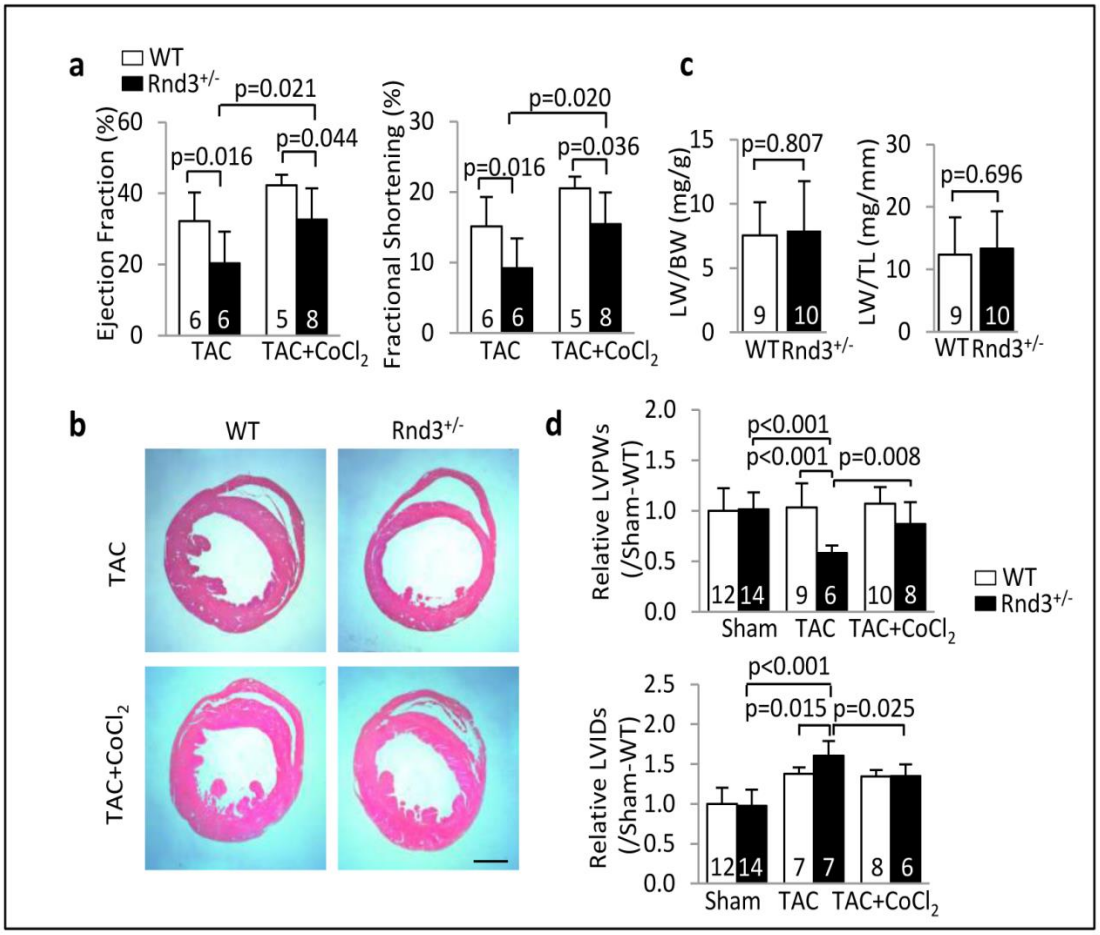

The HIF1α and VEGFA protein levels were compared in the WT and $Rnd3^{+/-}$ heart before and after TAC, with or without $CoCl_2$ treatment. Consistent with the previous result, $Rnd3^{+/-}$ heart displayed the significantly repressed HIF1α signaling after TAC. The $CoCl_2$ application stimulated HIF1α protein accumulation dramatically in the $Rnd3^{+/-}$ hearts compared with the non-treatment group. Along with the changes in HIF1α, significant increases in VEGFA protein levels were detected in the $Rnd3^{+/-}$ hearts with $CoCl_2$ treatment (Figure 15a), indicative of the rescued pro-angiogenic signaling pathway. To verify that $CoCl_2$ improved the responsive angiogenesis in Rnd3 deficient heart, capillary density and circulational perfusion were detected. Again, I observed the increased capillary number and area as well as the improved coronary flow reserve in the post-TAC $Rnd3^{+/-}$ hearts after $CoCl_2$ treatment, determined by the histological analysis and Doppler measured blood flow (Figure 15b to d).

In the animal study, Rnd3 deficiency resulted in heart failure and responsive angiogenesis associated with compromised HIF1-VEGFA signaling pathway. $CoCl_2$ partially rescued the adaptive vascularization in the $Rnd3^{+/-}$ heart via the compensated HIF1-VEGFA signaling pathway, therefore partially attenuated the cardiac dysfunction and the dilated cardiomyopathy phenotype. Rnd3 is a novel pro-angiogenesis factor that can binds to and stabilizes HIF1α protein. This novel discovery may provide a new strategy to the clinical therapy for the heart failure patients.

Figure 15. Responsive Angiogenesis Defect in the Post-TAC Rnd3$^{+/-}$ Heart was Partially Rescued by $CoCl_2$ Treatment. (a) The depressed HIF1α-VEGFA axis in post-TAC Rnd3$^{+/-}$ heart was raised by $CoCl_2$ application. (b) Isolectin-B4 stained cardiac capillaries (green) in $CoCl_2$ treated WT and Rnd3$^{+/-}$ post-TAC hearts. Nucleuses were visualized by blue DAPI staining. (c) Capillary areas and numbers from WT and Rnd3$^{+/-}$ hearts before and after surgery with or without $CoCl_2$ treatment were compared among groups. $CoCl_2$ significantly improved angiogenesis in Rnd3$^{+/-}$ hearts after TAC. (d) The impaired coronary flow reserve in Rnd3$^{+/-}$ heart was partially improved with $CoCl_2$ treatment. The number in each column represents animal numbers in each group. One-way ANOVA followed by Student-Newman-Keuls test was used for multiple group comparisons. The p value < 0.05 was considered as significant difference. Data are presented as means ± s.d.

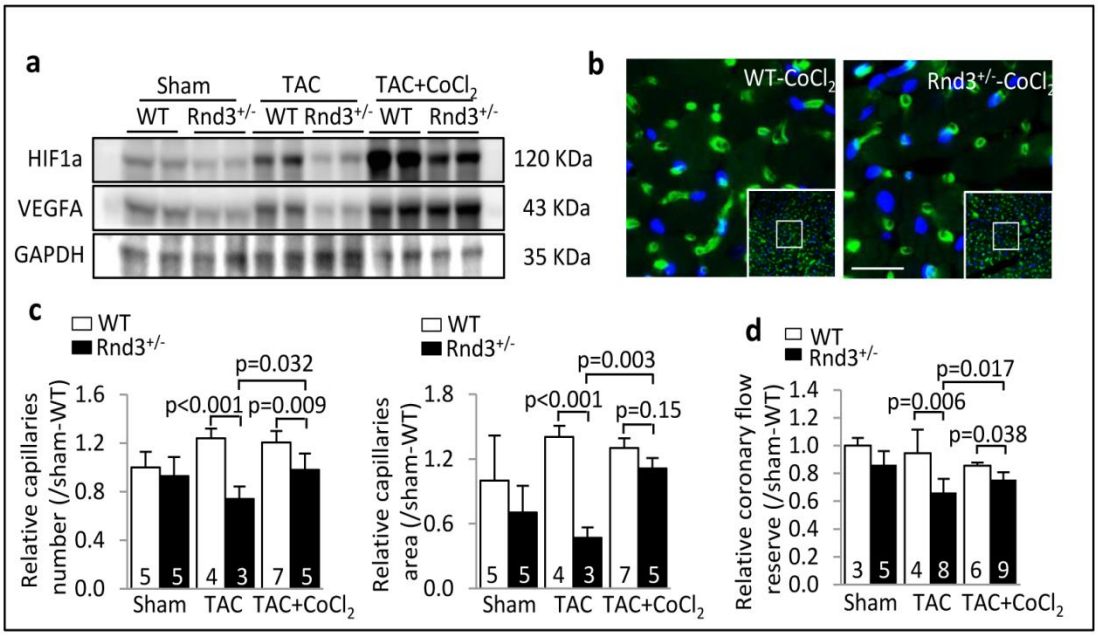

CHAPTER IV

CONCLUSIONS AND DISCUSSION

Rnd3, a constitutive active small Rho GTPase, mediates diversified cell stress response, such as DNA damage induced by chemotherapeutic agents or UVB exposure[50, 51]. Its expression level varies significantly upon cell differentiation during development and under stress, suggesting a delicate regulation of Rnd3 signaling is critical in pathophysiology[121]. The down-regulation of Rnd3 protein and mRNA levels were detected in end stage human failing hearts in my study and previous reports, suggesting that Rnd3 might play a role in the transition of the heart to failure. This study, so far, is the first one that investigates the role of Rnd3 in regulating heart failure under hemodynamic stress. Loss of Rnd3 in mouse myocardium resulted in severe apoptosis and impaired responsive angiogenesis induced by TAC compared to wild type littermates. Along with the massive apoptosis, ROCK1 signaling and Caspase3 were activated in the myocardium. My data suggested that the activated ROCK1 and Caspase3 are at least partially responsible for the cell death. Since ROCK1 inhibitor, Fasudil, or genetic deletion of *ROCK1* can significantly attenuate the apoptotic cardiomyopathy and sequentially recover the heart function. My study further confirmed the regulatory effect of Rnd3 on ROCK1 signaling in the heart, and provided a new candidate gene for new drug development targeting apoptotic cardiomyopathy. Whereas inhibition of ROCK1 could only partially rescue apoptosis and cardiac remodeling, suggesting that a ROCK1 independent pathway may exist. My further study investigated

the underlying mechanism and found that the compromised HIF1α-VEGFA signaling pathway mediated the angiogenesis defect in the Rnd3$^{+/-}$ heart and was responsible for the pathological changes. For the first time, my study demonstrated that Rnd3 physically binds to HIF1α and stabilizes it in the nucleus, resulting in its downstream angiogenesis pathway activation. Administration of cobalt chloride significantly rescued the down-regulation of HIF1α-VEGFA in the Rnd3$^{+/-}$ heart and attenuated the angiogenesis defect-mediated heart dysfunction. My study demonstrated a novel regulatory mechanism of angiogenesis in the hemodynamic stress exposed heart and provided a new potential strategy for therapeutic angiogenesis.

Role of Rnd3 in Apoptosis

Loss of Rnd3 induced cell death has been studied in different cell types. Rnd3 is a p53 target gene, and inhibits ROCK1-mediated apoptosis in response to genotoxic stress in many cell lines[46]. However, in U87 and keratinocytes, down-regulation of Rnd3 induced apoptosis appears more involved in the regulation of the ERK and p38 pro-survival pathway[122, 123], while in prostate cancer cell lines, its effect on cell apoptosis is closely associated with cell cycle regulation[124]. Interestingly, as a major event after myocardial infarction and many other heart diseases, the role of Rnd3 in cardiomyocyte apoptosis is poorly studied. Two major questions need to be answered: Does Rnd3 protect cardiomyocytes from apoptosis? How does Rnd3 regulate cardiomyocyte behavior after stress? This study showed that loss of Rnd3 triggered stronger apoptotic signaling after TAC. Rnd3 deficiency-mediated apoptosis is Rho Kinase dependent partially.

Role of Rnd3 in Heart End Stress

Hemodynamic stress induces significant cardiac remodeling. Our previous study showed that mice with overexpression of truncated ROCK1 are predisposed to angiotensin II induced cardiac fibrosis[43]. Since studies have shown that Rnd3 is a ROCK1 endogenous inhibitor[45], loss of Rnd3 should potentiate ROCK1 signaling. However, I did not see a significant difference in ROCK1 activity between the WT and the heterozygous Rnd3 mice. While under TAC induced stress condition, ROCK1 activity increased dramatically compared to the WT littermates, suggesting that the inhibition of ROCK1 by Rnd3 in heterozygous heart is a stress responsive process. Due to the embryonic lethality, further study focusing on the Rnd3 regulatory effect on ROCK1 in physiological condition should be conducted by using conditional Rnd3 knockout mice. It is also one of our on-going projects.

Caspase3 and Rho Kinase Activation in Apoptosis

ROCK1 has been shown to be closely associated with heart diseases, such as hypertension and fibrosis[43, 125, 126, 127]. Our previous study suggested that activation of ROCK1 by caspase3 cleavage played an essential role in cardiac apoptosis[42]. Apoptotic signals activated caspase 3, which can cleave ROCK1 resulting in a constitutive active ROCK1 isoform. The active ROCK1, on one hand, phosphorylated PTEN, which inhibited the pro-survival Akt pathway. On the other hand, the role of ROCK1 in apoptosis may be through the regulation of actin assembly to activate programed cell death signaling[128, 129, 130]. Specific Rho kinase 1 inhibitor development is still a challenge.

Rnd3 can only bind to ROCK1 but not ROCK2, providing a good drug candidate for specific targeting of ROCK1 signaling. My data suggests that the inhibition of ROCK1 only partially rescued the apoptosis, indicating other signals participate in Rnd3-mediated apoptosis (Figure 16). Investigation of Rnd3 mediated apoptosis independent of ROCK1 becomes interesting. The $Rnd3^{+/-ROCK1-/-}$ mouse line could be a great tool for this purpose. Rnd3 expression is dynamically regulated by different stresses, and it is also a target gene of p53. These provide the possibility that development of a specific compound could regulate Rnd3 expression without any modification of chromosomes. It is also possible that we can control patients' ROCK1 activities by modify Rnd3 expression with new development of Rnd3 agonists.

Figure 16. Mechanisms in the Rnd3 Mediated Heart Failure.

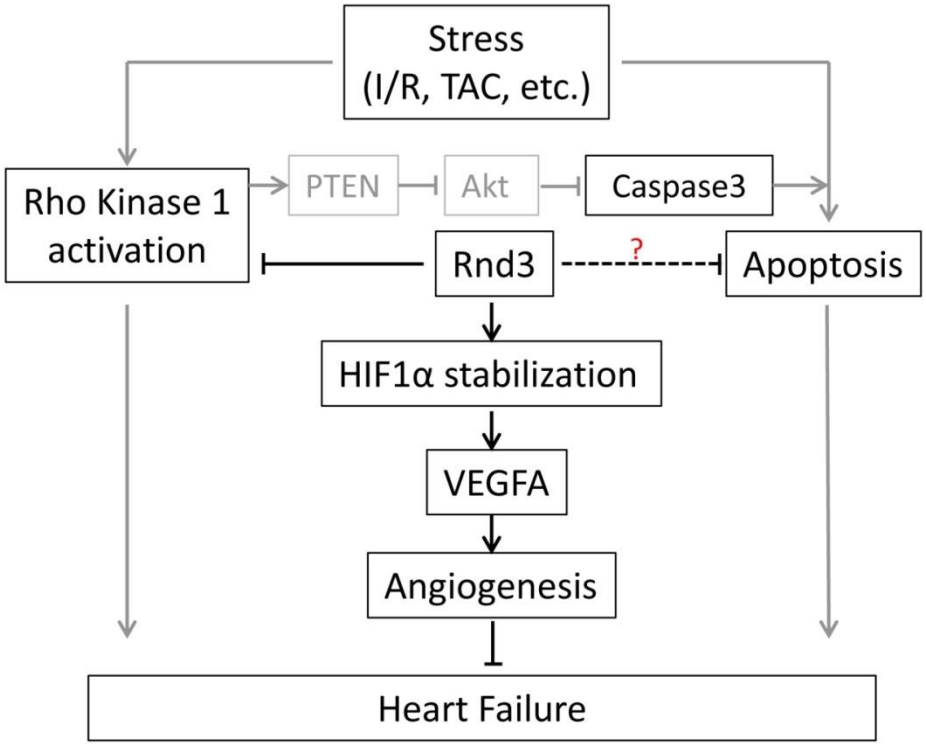

Fasudil and Cardiovascular Disease

Fasudil, targeting at the ATP-dependent kinase domain, is a commonly used ROCK inhibitor[25, 131]. Fasudil was widely used in ROCK study on cardiovascular disease, and functions as a vasodilator because of ROCK's regulation on smooth muscle contractility. Animal experiments showed Fasudil prevented ROCK-dependent hypertension[34, 132], atherosclerosis[133, 134], pulmonary hypertension[135, 136, 137], stroke[138] and myocardial infarction[139, 140]. In Japan, Fasudil was approved in 1995 for the treatment of cerebral vasospasm, which is the only clinical used ROCK inhibitor. Nowadays, the clinical trials

of Fasudil's therapeutical effects on cardiovascular disease, such as coronary artery disease[141], angina[142, 143, 144], pulmonary arterial hypertension[145, 146, 147] and stroke[148], are ongoing in different countries[15].

Although Fasudil reduced blood pressure in many pulmonary arterial hypertension models, the application of Fasudil in WT and $Rnd3^{+/-}$ mice did not result in blood pressure change. The non-specific inhibitory effects of Fasudil on other serine/ threonine kinases, such as PKA and PKC, have been reported at high dosage treatment[15, 149]. To minimize any possible side effects of Fasudil and also to verify the ROCK1's potential mechanism in Rnd3-mediated apoptotic cardiomyopathy, I generated the mice with the *Rnd3* and *ROCK1* double knockout background. Consistent with the rescue effects of Fasudil on the cardiac phenotype, loss of *ROCK1* gene also attenuated apoptotic cardiomyopathy partially. The data provided explicit evidence that Rnd3-mediated apoptotic cardiomyopathy is partially through a ROCK1-dependent pathway.

Role of Rnd3 in Angiogenesis

Early studies have reported that impaired cardiac capillary circulation led to heart failure. The patients with dilated cardiomyopathy suffered from left ventricle dysfunction associated with compromised myocardial perfusion, suggesting that abnormal cardiac perfusion plays a vital role in the development of heart to failure[150, 151, 152, 153]. CFR, the ratio of coronary flow velocity under stimuli and basal conditions, served as an index of coronary microvasculature. Cardiac angiogenesis was stimulated by hemodynamic

pressure overload with increased capillary density and CFR as the WT heart showed after TAC. However this compensatory response was insufficient in the $Rnd3^{+/-}$ heart and consequently resulted in pathological transition. The $Rnd3^{+/-}$ mice recapitulated the situations observed in human heart failure patients and is a novel disease-relevant mouse model.

Compromised HIF1α-VEGFA Signaling in Ischemic Heart

HIF1α mediated up-regulation of pro-angiogenic factors are critical in ischemia induced adaptive angiogenesis. HIF1α accumulation was detected in human hearts with ischemic stress[154]. In the mouse model in response to TAC stress, HIF1α and VEGFA were found to be activated within one week, but were decreased during days 14 to 28 along with cardiac remodeling and dysfunction. The patterns of HIF1α expression and angiogenesis were dynamic in the transition of the heart to failure[155]. Since cardiomyocytes are the major resource of VEGFA in the heart, the effect of cardiomyocyte-specific HIF1α on angiogenesis was investigated. Knockout of HIF1α in mouse cardiomycytes was proven to contribute to baseline poor vasculature and cardiac dysfunction[156]. Cardiac-specific knockout of HIF1α from one allele resulted in an angiogenesis defect and cardiac contractile dysfunction after TAC[155].

The $Rnd3^{+/-}$ mouse line is a novel model for angiogenesis study. Under basal condition, $Rnd3^{+/-}$ mice developed normal cardiac angiogenesis with similar capillary density, coronary flow reserve and HIF1α-VEGFA levels compared with the WT control. Under

hemodynamic stress challenge condition, the activated HIF1α-VEGFA pathway was detected in the WT heart, whereas failed HIF1α-VEGFA compensation was detected in the $Rnd3^{+/-}$ heart, resulting in the failure of adaptive angiogenesis indicated by low capillary density and reduced coronary flow reserve. Consistent with the phenotype exhibited in $Rnd3^{+/-}$ mice, an endothelial cell tube formation assay using cardiomyocyte conditional medium demonstrated that $Rnd3^{+/-}$ cardiomyocytes secreted less VEGFA compared with the WT control. The repressed HIF1α-VEGFA signaling is responsible for the angiogenesis defect mediated transition of the heart to failure.

Cobalt chloride stabilizes HIF1α by inhibiting PHD[157]. To verify the HIF1α-VEGFA regulatory axis in the Rnd3 deficiency mediated angiogenesis defect, cobalt chloride was applied as a mouse heart failure precondition treatment. In the TAC stress exposed $Rnd3^{+/-}$ heart, the administration of cobalt chloride stimulated capillary generation, improved myocardial perfusion, rescued left ventricle dilation and promoted cardiac function. The compromised HIF1α-VEGFA pathway in the $Rnd3^{+/-}$ heart was also rescued by cobalt chloride application. Interestingly, although cobalt chloride has an effect on WT and $Rnd3^{+/-}$ mice and stimulated HIF1α accumulation, the WT heart exhibited much higher levels of HIF1α compared with the mutant heart. The VEGFA levels were greatly induced, however, did not show significant difference between the two groups after cobalt chloride treatment. This situation indicated that stabilization of HIF1α promoted VEGFA mediated angiogenesis and rescued dilated cardiomyopathy in the Rnd3 deficient heart, whereas high doses of HIF1α probably cannot further push the

VEGFA expression, which suggests other potential mechanisms regulating the VEGFA pathway.

Rnd3-HIF1α Regulation Loop

HIF1α is a ubiquitously expressed oxygen sensor protein. In normoxia, HIF1α stays in the cytoplasm and is degraded by 26S proteasome after binding with ubiquitin E3 ligase VHL. The *in vivo* data showed that HIF1α protein levels decreased in the Rnd3 mutant heart after TAC stimuli, and our loss- and gain-of-function experiments further demonstrated that Rnd3 facilitated HIF1α protein accumulation in the nucleus, suggesting that Rnd3 plays a regulatory role in HIF1α protein turnover. An immunoprecipitation experiment demonstrated that Rnd3 physically bound to HIF1α protein. Therefore, I proposed a novel angiogenesis regulatory mechanism that Rnd3 binds to and stabilizes HIF1α and consequently enhances the VEGFA mediated angiogenesis pathway (Figure 17). On the other hand, Rnd3 probably is regulated by HIF1α at the transcriptional level as a feedback regulation loop. HIF1α was found to interact with the HRE element in the *Rnd3* gene promoter region during hypoxia, and was associated with the up-regulation of Rnd3 in response to hypoxia stimuli[158]. Given the vital role of HIF1α in angiogenesis, Rnd3 may function as a new positive regulator and activation of Rnd3 may be an attractive option in therapeutic angiogenesis.

Figure 17. Proposed Model of the Molecular Mechanism of Rnd3 in Angiogenesis. Rnd3 interacts and stabilizes HIF1α facilitating the activation of VEGF transcription in nuclei. The HIF1α monomer is quickly degraded by UPS system after the hydroxylation modification by enzyme PHD under normoxia condition. The hydroxylation can be blocked by cobalt chloride. UPS: ubiquitin-proteasome system; PHD: prolyl hydroxylase domain.

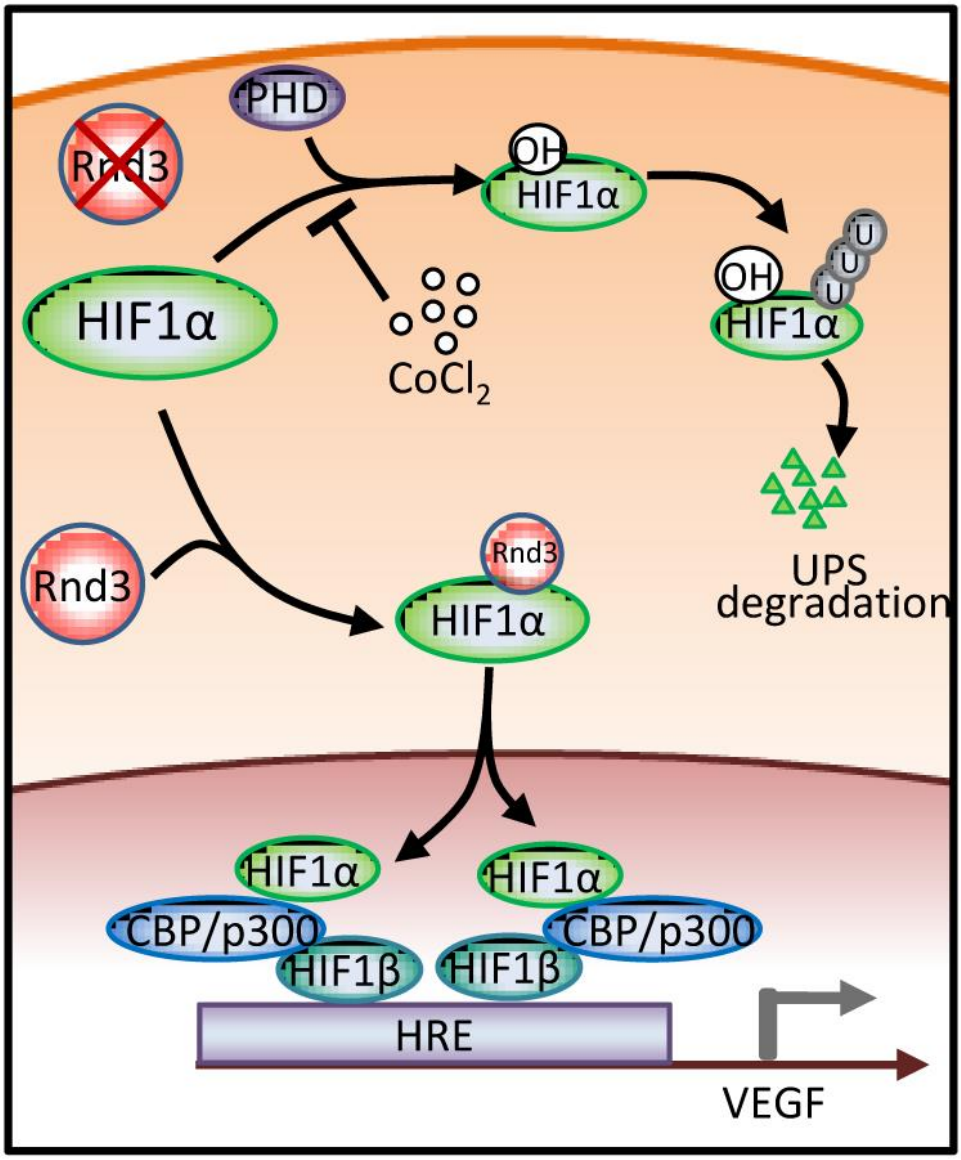

REFERENCES

1. Go AS, Mozaffarian D, Roger VL, Benjamin EJ, Berry JD, Blaha MJ, *et al.* Heart disease and stroke statistics--2014 update: a report from the American Heart Association. *Circulation* 2014, **129**(3)**:** e28-e292.

2. Roger VL, Go AS, Lloyd-Jones DM, Adams RJ, Berry JD, Brown TM, *et al.* Heart disease and stroke statistics--2011 update: a report from the American Heart Association. *Circulation* 2011, **123**(4)**:** e18-e209.

3. Richardson P, McKenna W, Bristow M, Maisch B, Mautner B, O'Connell J, *et al.* Report of the 1995 World Health Organization/International Society and Federation of Cardiology Task Force on the definition and classification of cardiomyopathies. *Circulation* 1996, **93**(5)**:** 841-842.

4. Elliott P, Andersson B, Arbustini E, Bilinska Z, Cecchi F, Charron P, *et al.* Classification of the cardiomyopathies: a position statement from the European Society Of Cardiology working group on myocardial and pericardial diseases. *Eur Heart J* 2008, **29**(2)**:** 270-276.

5. Maron BJ, Towbin JA, Thiene G, Antzelevitch C, Corrado D, Arnett D, *et al.* Contemporary definitions and classification of the cardiomyopathies: an American Heart Association scientific statement from the council on clinical cardiology, heart failure and transplantation committee; quality of care and outcomes research and functional genomics and translational biology interdisciplinary working groups; and council on epidemiology and prevention. *Circulation* 2006, **113**(14)**:** 1807-1816.

6. Louie EK, Maron BJ. Hypertrophic cardiomyopathy with extreme increase in left ventricular wall thickness: functional and morphologic features and clinical significance. *J Am Coll Cardiol* 1986, **8**(1)**:** 57-65.

7. Spirito P, Bellone P, Harris KM, Bernabo P, Bruzzi P, Maron BJ. Magnitude of left ventricular hypertrophy and risk of sudden death in hypertrophic cardiomyopathy. *N Engl J Med* 2000, **342**(24)**:** 1778-1785.

8. Maron BJ, Maron MS. Hypertrophic cardiomyopathy. *Lancet* 2013, **381**(9862)**:** 242-255.

9. Maron BJ, Haas TS, Kitner C, Lesser JR. Onset of apical hypertrophic cardiomyopathy in adulthood. *Am J Cardiol* 2011, **108**(12)**:** 1783-1787.

10. Luk A, Ahn E, Soor GS, Butany J. Dilated cardiomyopathy: a review. *J Clin Pathol* 2009, **62**(3)**:** 219-225.

11. Matsui T, Amano M, Yamamoto T, Chihara K, Nakafuku M, Ito M, *et al.* Rho-associated kinase, a novel serine/threonine kinase, as a putative target for small GTP binding protein Rho. *EMBO J* 1996, **15**(9)**:** 2208-2216.

12. Ishizaki T, Maekawa M, Fujisawa K, Okawa K, Iwamatsu A, Fujita A, *et al.* The small GTP-binding protein Rho binds to and activates a 160 kDa Ser/Thr protein kinase homologous to myotonic dystrophy kinase. *EMBO J* 1996, **15**(8)**:** 1885-1893.

13. Leung T, Chen XQ, Manser E, Lim L. The p160 RhoA-binding kinase ROK alpha is a member of a kinase family and is involved in the reorganization of the cytoskeleton. *Mol Cell Biol* 1996, **16**(10)**:** 5313-5327.

14. Nakagawa O, Fujisawa K, Ishizaki T, Saito Y, Nakao K, Narumiya S. ROCK-I and ROCK-II, two isoforms of Rho-associated coiled-coil forming protein serine/threonine kinase in mice. *FEBS Lett* 1996, **392**(2)**:** 189-193.

15. Shi J, Wei L. Rho kinases in cardiovascular physiology and pathophysiology: the effect of fasudil. *J Cardiovasc Pharmacol* 2013, **62**(4)**:** 341-354.

16. Kureishi Y, Kobayashi S, Amano M, Kimura K, Kanaide H, Nakano T, *et al.* Rho-associated kinase directly induces smooth muscle contraction through myosin light chain phosphorylation. *J Biol Chem* 1997, **272**(19)**:** 12257-12260.

17. Kimura K, Ito M, Amano M, Chihara K, Fukata Y, Nakafuku M, *et al.* Regulation of myosin phosphatase by Rho and Rho-associated kinase (Rho-kinase). *Science* 1996, **273**(5272)**:** 245-248.

18. Amano M, Ito M, Kimura K, Fukata Y, Chihara K, Nakano T, *et al.* Phosphorylation and activation of myosin by Rho-associated kinase (Rho-kinase). *J Biol Chem* 1996, **271**(34)**:** 20246-20249.

19. Maekawa M, Ishizaki T, Boku S, Watanabe N, Fujita A, Iwamatsu A, *et al.* Signaling from Rho to the actin cytoskeleton through protein kinases ROCK and LIM-kinase. *Science* 1999, **285**(5429)**:** 895-898.

20. Ohashi K, Nagata K, Maekawa M, Ishizaki T, Narumiya S, Mizuno K. Rho-associated kinase ROCK activates LIM-kinase 1 by phosphorylation at threonine 508 within the activation loop. *J Biol Chem* 2000, **275**(5)**:** 3577-3582.

21. Amano T, Tanabe K, Eto T, Narumiya S, Mizuno K. LIM-kinase 2 induces formation of stress fibres, focal adhesions and membrane blebs, dependent on its activation by Rho-associated kinase-catalysed phosphorylation at threonine-505. *Biochem J* 2001, **354**(Pt 1)**:** 149-159.

22. Sumi T, Matsumoto K, Nakamura T. Specific activation of LIM kinase 2 via phosphorylation of threonine 505 by ROCK, a Rho-dependent protein kinase. *J Biol Chem* 2001, **276**(1)**:** 670-676.

23. Matsui T, Maeda M, Doi Y, Yonemura S, Amano M, Kaibuchi K, *et al.* Rho-kinase phosphorylates COOH-terminal threonines of ezrin/radixin/moesin (ERM) proteins and regulates their head-to-tail association. *J Cell Biol* 1998, **140**(3)**:** 647-657.

24. Fukata Y, Oshiro N, Kinoshita N, Kawano Y, Matsuoka Y, Bennett V, *et al.* Phosphorylation of adducin by Rho-kinase plays a crucial role in cell motility. *J Cell Biol* 1999, **145**(2)**:** 347-361.

25. Uehata M, Ishizaki T, Satoh H, Ono T, Kawahara T, Morishita T, *et al.* Calcium sensitization of smooth muscle mediated by a Rho-associated protein kinase in hypertension. *Nature* 1997, **389**(6654)**:** 990-994.

26. Coleman ML, Sahai EA, Yeo M, Bosch M, Dewar A, Olson MF. Membrane blebbing during apoptosis results from caspase-mediated activation of ROCK I. *Nat Cell Biol* 2001, **3**(4)**:** 339-345.

27. Vigil D, Kim TY, Plachco A, Garton AJ, Castaldo L, Pachter JA, *et al.* ROCK1 and ROCK2 are required for non-small cell lung cancer anchorage-independent growth and invasion. *Cancer Res* 2012, **72**(20)**:** 5338-5347.

28. Inaba N, Ishizawa S, Kimura M, Fujioka K, Watanabe M, Shibasaki T, *et al.* Effect of inhibition of the ROCK isoform on RT2 malignant glioma cells. *Anticancer Res* 2010, **30**(9)**:** 3509-3514.

29. Wang Y, Zheng XR, Riddick N, Bryden M, Baur W, Zhang X, *et al.* ROCK isoform regulation of myosin phosphatase and contractility in vascular smooth muscle cells. *Circ Res* 2009, **104**(4)**:** 531-540.

30. Zhao Y, Lv M, Lin H, Hong Y, Yang F, Sun Y, *et al.* ROCK1 induces ERK nuclear translocation in PDGF-BB-stimulated migration of rat vascular smooth muscle cells. *IUBMB Life* 2012, **64**(2)**:** 194-202.

31. Seasholtz TM, Majumdar M, Kaplan DD, Brown JH. Rho and Rho kinase mediate thrombin-stimulated vascular smooth muscle cell DNA synthesis and migration. *Circ Res* 1999, **84**(10)**:** 1186-1193.

32. Kamiyama M, Utsunomiya K, Taniguchi K, Yokota T, Kurata H, Tajima N, *et al.* Contribution of Rho A and Rho kinase to platelet-derived growth factor-BB-induced proliferation of vascular smooth muscle cells. *J Atheroscler Thromb* 2003, **10**(2)**:** 117-123.

33. Mukai Y, Shimokawa H, Matoba T, Kandabashi T, Satoh S, Hiroki J, *et al.* Involvement of Rho-kinase in hypertensive vascular disease: a novel therapeutic target in hypertension. *FASEB J* 2001, **15**(6)**:** 1062-1064.

34. Tsounapi P, Saito M, Kitatani K, Dimitriadis F, Ohmasa F, Shimizu S, *et al.* Fasudil improves the endothelial dysfunction in the aorta of spontaneously hypertensive rats. *Eur J Pharmacol* 2012, **691**(1-3)**:** 182-189.

35. Rolfe BE, Worth NF, World CJ, Campbell JH, Campbell GR. Rho and vascular disease. *Atherosclerosis* 2005, **183**(1)**:** 1-16.

36. Gorovoy M, Niu J, Bernard O, Profirovic J, Minshall R, Neamu R, *et al.* LIM kinase 1 coordinates microtubule stability and actin polymerization in human endothelial cells. *J Biol Chem* 2005, **280**(28)**:** 26533-26542.

37. Birukova AA, Smurova K, Birukov KG, Usatyuk P, Liu F, Kaibuchi K, *et al.* Microtubule disassembly induces cytoskeletal remodeling and lung vascular barrier dysfunction: role of Rho-dependent mechanisms. *J Cell Physiol* 2004, **201**(1)**:** 55-70.

38. Bryan BA, Dennstedt E, Mitchell DC, Walshe TE, Noma K, Loureiro R, *et al.* RhoA/ROCK signaling is essential for multiple aspects of VEGF-mediated angiogenesis. *FASEB J* 2010, **24**(9)**:** 3186-3195.

39. Cattan CE, Oberg KC. Vinorelbine tartrate-induced pulmonary edema confirmed on rechallenge. *Pharmacotherapy* 1999, **19**(8)**:** 992-994.

40. Noma K, Rikitake Y, Oyama N, Yan G, Alcaide P, Liu PY, *et al.* ROCK1 mediates leukocyte recruitment and neointima formation following vascular injury. *J Clin Invest* 2008, **118**(5)**:** 1632-1644.

41. Mallat Z, Gojova A, Sauzeau V, Brun V, Silvestre JS, Esposito B, *et al.* Rho-associated protein kinase contributes to early atherosclerotic lesion formation in mice. *Circ Res* 2003, **93**(9)**:** 884-888.

42. Chang J, Xie M, Shah VR, Schneider MD, Entman ML, Wei L, *et al.* Activation of Rho-associated coiled-coil protein kinase 1 (ROCK-1) by caspase-3 cleavage plays an essential role in cardiac myocyte apoptosis. *Proc Natl Acad Sci U S A* 2006, **103**(39)**:** 14495-14500.

43. Yang X, Li Q, Lin X, Ma Y, Yue X, Tao Z, *et al.* Mechanism of fibrotic cardiomyopathy in mice expressing truncated Rho-associated coiled-coil protein kinase 1. *FASEB J* 2012, **26**(5)**:** 2105-2116.

44. Sebbagh M, Renvoize C, Hamelin J, Riche N, Bertoglio J, Breard J. Caspase-3-mediated cleavage of ROCK I induces MLC phosphorylation and apoptotic membrane blebbing. *Nat Cell Biol* 2001, **3**(4)**:** 346-352.

45. Riento K, Guasch RM, Garg R, Jin B, Ridley AJ. RhoE binds to ROCK I and inhibits downstream signaling. *Mol Cell Biol* 2003, **23**(12)**:** 4219-4229.

46. Ongusaha PP, Kim HG, Boswell SA, Ridley AJ, Der CJ, Dotto GP, *et al.* RhoE is a pro-survival p53 target gene that inhibits ROCK I-mediated apoptosis in response to genotoxic stress. *Curr Biol* 2006, **16**(24)**:** 2466-2472.

47. Komander D, Garg R, Wan PT, Ridley AJ, Barford D. Mechanism of multi-site phosphorylation from a ROCK-I:RhoE complex structure. *EMBO J* 2008, **27**(23)**:** 3175-3185.

48. Pinner S, Sahai E. PDK1 regulates cancer cell motility by antagonising inhibition of ROCK1 by RhoE. *Nature Cell Biology* 2008, **10**(2)**:** 127-137.

49. Foster R, Hu KQ, Lu Y, Nolan KM, Thissen J, Settleman J. Identification of a novel human Rho protein with unusual properties: GTPase deficiency and in vivo farnesylation. *Mol Cell Biol* 1996, **16**(6)**:** 2689-2699.

50. Shurin GV, Tourkova IL, Shurin MR. Low-dose chemotherapeutic agents regulate small Rho GTPase activity in dendritic cells. *J Immunother* 2008, **31**(5)**:** 491-499.

51. Boswell SA, Ongusaha PP, Nghiem P, Lee SW. The protective role of a small GTPase RhoE against UVB-induced DNA damage in keratinocytes. *J Biol Chem* 2007, **282**(7)**:** 4850-4858.

52. Nadiminty N, Dutt S, Tepper C, Gao AC. Microarray analysis reveals potential target genes of NF-kappaB2/p52 in LNCaP prostate cancer cells. *Prostate* 2010, **70**(3)**:** 276-287.

53. Tyburczy ME, Kotulska K, Pokarowski P, Mieczkowski J, Kucharska J, Grajkowska W, *et al.* Novel proteins regulated by mTOR in subependymal giant cell astrocytomas of patients with tuberous sclerosis complex and new therapeutic implications. *The American Journal of Pathology* 2010, **176**(4)**:** 1878-1890.

54. Hurteau GJ, Spivack SD, Brock GJ. Potential mRNA degradation targets of hsa-miR-200c, identified using informatics and qRT-PCR. *Cell Cycle* 2006, **5**(17)**:** 1951-1956.

55. Riento K, Totty N, Villalonga P, Garg R, Guasch R, Ridley AJ. RhoE function is regulated by ROCK I-mediated phosphorylation. *EMBO J* 2005, **24**(6)**:** 1170-1180.

56. Madigan JP, Bodemann BO, Brady DC, Dewar BJ, Keller PJ, Leitges M, *et al.* Regulation of Rnd3 localization and function by protein kinase C alpha-mediated phosphorylation. *The Biochemical Journal* 2009, **424**(1)**:** 153-161.

57. Riou P, Kjaer S, Garg R, Purkiss A, George R, Cain RJ, *et al.* 14-3-3 proteins interact with a hybrid prenyl-phosphorylation motif to inhibit g proteins. *Cell* 2013, **153**(3)**:** 640-653.

58. Guasch RM, Scambler P, Jones GE, Ridley AJ. RhoE regulates actin cytoskeleton organization and cell migration. *Mol Cell Biol* 1998, **18**(8)**:** 4761-4771.

59. Lartey J, Gampel A, Pawade J, Mellor H, Bernal AL. Expression of RND proteins in human myometrium. *Biol Reprod* 2006, **75**(3)**:** 452-461.

60. Cario-Toumaniantz C, Reillaudoux G, Sauzeau V, Heutte F, Vaillant N, Finet M, *et al.* Modulation of RhoA-Rho kinase-mediated Ca^{2+} sensitization of rabbit myometrium during pregnancy - role of Rnd3. *The Journal of Physiology* 2003, **552**(Pt 2)**:** 403-413.

61. Bektic J, Pfeil K, Berger AP, Ramoner R, Pelzer A, Schafer G, *et al.* Small G-protein RhoE is underexpressed in prostate cancer and induces cell cycle arrest and apoptosis. *Prostate* 2005, **64**(4)**:** 332-340.

62. Klein RM, Aplin AE. Rnd3 regulation of the actin cytoskeleton promotes melanoma migration and invasive outgrowth in three dimensions. *Cancer Res* 2009, **69**(6)**:** 2224-2233.

63. Akashi H, Han HJ, Iizaka M, Nakamura Y. Growth-suppressive effect of non-steroidal anti-inflammatory drugs on 11 colon-cancer cell lines and fluorescence differential display of genes whose expression is influenced by sulindac. *Int J Cancer* 2000, **88**(6)**:** 873-880.

64. Gress TM, Muller-Pillasch F, Geng M, Zimmerhackl F, Zehetner G, Friess H, *et al.* A pancreatic cancer-specific expression profile. *Oncogene* 1996, **13**(8)**:** 1819-1830.

65. Mocholi E, Ballester-Lurbe B, Arque G, Poch E, Peris B, Guerri C, *et al.* RhoE deficiency produces postnatal lethality, profound motor deficits and neurodevelopmental delay in mice. *PLoS One* 2011, **6**(4)**:** e19236.

66. Li J, Anton ES. Rnd-ing up RhoA activity to link neurogenesis with steps in neuronal migration. *Dev Cell* 2011, **20**(4)**:** 409-410.

67. Pacary E, Heng J, Azzarelli R, Riou P, Castro D, Lebel-Potter M, *et al.* Proneural transcription factors regulate different steps of cortical neuron migration through Rnd-mediated inhibition of RhoA signaling. *Neuron* 2011, **69**(6)**:** 1069-1084.

68. Lin X, Liu B, Yang X, Yue X, Diao L, Wang J, *et al.* Genetic deletion of Rnd3 results in aqueductal stenosis leading to hydrocephalus through up-regulation of Notch signaling. *Proc Natl Acad Sci U S A* 2013, **110**(20)**:** 8236-8241.

69. Yang X, Wang T, Lin X, Yue X, Wang Q, Wang G, *et al.* Genetic deletion of Rnd3/RhoE results in mouse heart calcium leakage through upregulation of protein kinase A signaling. *Circ Res* 2015, **116**(1)**:** e1-e10.

70. Olson EN, Schneider MD. Sizing up the heart: development redux in disease. *Genes Dev* 2003, **17**(16)**:** 1937-1956.

71. Hudlicka O, Brown MD. Postnatal growth of the heart and its blood vessels. *J Vasc Res* 1996, **33**(4)**:** 266-287.

72. White FC, Bloor CM, McKirnan MD, Carroll SM. Exercise training in swine promotes growth of arteriolar bed and capillary angiogenesis in heart. *J Appl Physiol* 1998, **85**(3)**:** 1160-1168.

73. Duncker DJ, Bache RJ. Regulation of coronary blood flow during exercise. *Physiol Rev* 2008, **88**(3)**:** 1009-1086.

74. Tomanek RJ, Torry RJ. Growth of the coronary vasculature in hypertrophy: mechanisms and model dependence. *Cellular & Molecular Biology Research* 1994, **40**(2)**:** 129-136.

75. Matsunaga T, Warltier DC, Weihrauch DW, Moniz M, Tessmer J, Chilian WM. Ischemia-induced coronary collateral growth is dependent on vascular endothelial growth factor and nitric oxide. *Circulation* 2000, **102**(25)**:** 3098-3103.

76. Shiojima I, Sato K, Izumiya Y, Schiekofer S, Ito M, Liao R, *et al.* Disruption of coordinated cardiac hypertrophy and angiogenesis contributes to the transition to heart failure. *J Clin Invest* 2005, **115**(8)**:** 2108-2118.

77. Dorn GW, 2nd. Myocardial angiogenesis: its absence makes the growing heart founder. *Cell Metab* 2007, **5**(5)**:** 326-327.

78. Ferrara N, Carver-Moore K, Chen H, Dowd M, Lu L, O'Shea KS, *et al.* Heterozygous embryonic lethality induced by targeted inactivation of the VEGF gene. *Nature* 1996, **380**(6573)**:** 439-442.

79. Carmeliet P, Ferreira V, Breier G, Pollefeyt S, Kieckens L, Gertsenstein M, *et al.* Abnormal blood vessel development and lethality in embryos lacking a single VEGF allele. *Nature* 1996, **380**(6573)**:** 435-439.

80. Friesel RE, Maciag T. Molecular mechanisms of angiogenesis: fibroblast growth factor signal transduction. *FASEB J* 1995, **9**(10)**:** 919-925.

81. Davis S, Aldrich TH, Jones PF, Acheson A, Compton DL, Jain V, *et al.* Isolation of angiopoietin-1, a ligand for the TIE2 receptor, by secretion-trap expression cloning. *Cell* 1996, **87**(7)**:** 1161-1169.

82. Salani D, Taraboletti G, Rosano L, Di Castro V, Borsotti P, Giavazzi R, *et al.* Endothelin-1 induces an angiogenic phenotype in cultured endothelial cells and stimulates neovascularization in vivo. *Am J Pathol* 2000, **157**(5)**:** 1703-1711.

83. Bagnato A, Spinella F. Emerging role of endothelin-1 in tumor angiogenesis. *Trends Endocrinol Metab* 2003, **14**(1)**:** 44-50.

84. Wu MH, Huang CY, Lin JA, Wang SW, Peng CY, Cheng HC, *et al.* Endothelin-1 promotes vascular endothelial growth factor-dependent angiogenesis in human chondrosarcoma cells. *Oncogene* 2014, **33**(13)**:** 1725-1735.

85. Roberts AB, Sporn MB. Regulation of endothelial cell growth, architecture, and matrix synthesis by TGF-beta. *Am Rev Respir Dis* 1989, **140**(4)**:** 1126-1128.

86. Tabruyn SP, Griffioen AW. A new role for NF-kappaB in angiogenesis inhibition. *Cell Death Differ* 2007, **14**(8)**:** 1393-1397.

87. Dor Y, Djonov V, Abramovitch R, Itin A, Fishman GI, Carmeliet P, *et al.* Conditional switching of VEGF provides new insights into adult neovascularization and pro-angiogenic therapy. *EMBO J* 2002, **21**(8)**:** 1939-1947.

88. Cao R, Brakenhielm E, Pawliuk R, Wariaro D, Post MJ, Wahlberg E, *et al.* Angiogenic synergism, vascular stability and improvement of hind-limb ischemia by a combination of PDGF-BB and FGF-2. *Nat Med* 2003, **9**(5)**:** 604-613.

89. Post MJ, Laham R, Sellke FW, Simons M. Therapeutic angiogenesis in cardiology using protein formulations. *Cardiovasc Res* 2001, **49**(3)**:** 522-531.

90. Harada K, Friedman M, Lopez JJ, Wang SY, Li J, Prasad PV, *et al.* Vascular endothelial growth factor administration in chronic myocardial ischemia. *Am J Physiol* 1996, **270**(5 Pt 2)**:** H1791-1802.

91. Hendel RC, Henry TD, Rocha-Singh K, Isner JM, Kereiakes DJ, Giordano FJ, *et al.* Effect of intracoronary recombinant human vascular endothelial growth factor on myocardial perfusion: evidence for a dose-dependent effect. *Circulation* 2000, **101**(2)**:** 118-121.

92. Henry TD, Rocha-Singh K, Isner JM, Kereiakes DJ, Giordano FJ, Simons M, *et al.* Intracoronary administration of recombinant human vascular endothelial growth factor to patients with coronary artery disease. *Am Heart J* 2001, **142**(5)**:** 872-880.

93. Henry TD, Annex BH, McKendall GR, Azrin MA, Lopez JJ, Giordano FJ, *et al.* The VIVA trial: vascular endothelial growth factor in ischemia for vascular angiogenesis. *Circulation* 2003, **107**(10)**:** 1359-1365.

94. Kawasaki T, Kitsukawa T, Bekku Y, Matsuda Y, Sanbo M, Yagi T, *et al.* A requirement for neuropilin-1 in embryonic vessel formation. *Development* 1999, **126**(21)**:** 4895-4902.

95. Shibuya M, Ito N, Claesson-Welsh L. Structure and function of vascular endothelial growth factor receptor-1 and -2. *Curr Top Microbiol Immunol* 1999, **237:** 59-83.

96. Shalaby F, Rossant J, Yamaguchi TP, Gertsenstein M, Wu XF, Breitman ML, *et al.* Failure of blood-island formation and vasculogenesis in Flk-1-deficient mice. *Nature* 1995, **376**(6535)**:** 62-66.

97. Hoeben A, Landuyt B, Highley MS, Wildiers H, Van Oosterom AT, De Bruijn EA. Vascular endothelial growth factor and angiogenesis. *Pharmacol Rev* 2004, **56**(4)**:** 549-580.

98. Hicklin DJ, Ellis LM. Role of the vascular endothelial growth factor pathway in tumor growth and angiogenesis. *J Clin Oncol* 2005, **23**(5)**:** 1011-1027.

99. Mitsos S, Katsanos K, Koletsis E, Kagadis GC, Anastasiou N, Diamantopoulos A, *et al.* Therapeutic angiogenesis for myocardial ischemia revisited: basic biological concepts and focus on latest clinical trials. *Angiogenesis* 2012, **15**(1)**:** 1-22.

100. Senger DR, Van de Water L, Brown LF, Nagy JA, Yeo KT, Yeo TK, *et al.* Vascular permeability factor (VPF, VEGF) in tumor biology. *Cancer Metastasis Rev* 1993, **12**(3-4)**:** 303-324.

101. Banai S, Shweiki D, Pinson A, Chandra M, Lazarovici G, Keshet E. Upregulation of vascular endothelial growth factor expression induced by myocardial ischaemia: implications for coronary angiogenesis. *Cardiovasc Res* 1994, **28**(8)**:** 1176-1179.

102. Hashimoto E, Ogita T, Nakaoka T, Matsuoka R, Takao A, Kira Y. Rapid induction of vascular endothelial growth factor expression by transient ischemia in rat heart. *Am J Physiol* 1994, **267**(5 Pt 2)**:** H1948-1954.

103. Li J, Brown LF, Hibberd MG, Grossman JD, Morgan JP, Simons M. VEGF, flk-1, and flt-1 expression in a rat myocardial infarction model of angiogenesis. *Am J Physiol* 1996, **270**(5 Pt 2)**:** H1803-1811.

104. Pugh CW, Ratcliffe PJ. Regulation of angiogenesis by hypoxia: role of the HIF system. *Nat Med* 2003, **9**(6)**:** 677-684.

105. Arany Z, Foo SY, Ma Y, Ruas JL, Bommi-Reddy A, Girnun G, *et al.* HIF-independent regulation of VEGF and angiogenesis by the transcriptional coactivator PGC-1alpha. *Nature* 2008, **451**(7181)**:** 1008-1012.

106. Ke Q, Costa M. Hypoxia-inducible factor-1 (HIF-1). *Mol Pharmacol* 2006, **70**(5)**:** 1469-1480.

107. Masson N, Willam C, Maxwell PH, Pugh CW, Ratcliffe PJ. Independent function of two destruction domains in hypoxia-inducible factor-alpha chains activated by prolyl hydroxylation. *EMBO J* 2001, **20**(18)**:** 5197-5206.

108. Srinivas V, Zhang LP, Zhu XH, Caro J. Characterization of an oxygen/redox-dependent degradation domain of hypoxia-inducible factor alpha (HIF-alpha) proteins. *Biochem Biophys Res Commun* 1999, **260**(2)**:** 557-561.

109. Lando D, Peet DJ, Gorman JJ, Whelan DA, Whitelaw ML, Bruick RK. FIH-1 is an asparaginyl hydroxylase enzyme that regulates the transcriptional activity of hypoxia-inducible factor. *Genes Dev* 2002, **16**(12)**:** 1466-1471.

110. Epstein AC, Gleadle JM, McNeill LA, Hewitson KS, O'Rourke J, Mole DR, *et al.* C. elegans EGL-9 and mammalian homologs define a family of dioxygenases that regulate HIF by prolyl hydroxylation. *Cell* 2001, **107**(1)**:** 43-54.

111. Lando D, Peet DJ, Whelan DA, Gorman JJ, Whitelaw ML. Asparagine hydroxylation of the HIF transactivation domain a hypoxic switch. *Science* 2002, **295**(5556)**:** 858-861.

112. Crews ST. Control of cell lineage-specific development and transcription by bHLH-PAS proteins. *Genes Dev* 1998, **12**(5)**:** 607-620.

113. Hu CJ, Wang LY, Chodosh LA, Keith B, Simon MC. Differential roles of hypoxia-inducible factor 1alpha (HIF-1alpha) and HIF-2alpha in hypoxic gene regulation. *Mol Cell Biol* 2003, **23**(24)**:** 9361-9374.

114. Tang N, Wang L, Esko J, Giordano FJ, Huang Y, Gerber HP*, et al.* Loss of HIF-1alpha in endothelial cells disrupts a hypoxia-driven VEGF autocrine loop necessary for tumorigenesis. *Cancer Cell* 2004, **6**(5)**:** 485-495.

115. Hu CJ, Sataur A, Wang L, Chen H, Simon MC. The N-terminal transactivation domain confers target gene specificity of hypoxia-inducible factors HIF-1alpha and HIF-2alpha. *Mol Biol Cell* 2007, **18**(11)**:** 4528-4542.

116. Raval RR, Lau KW, Tran MG, Sowter HM, Mandriota SJ, Li JL*, et al.* Contrasting properties of hypoxia-inducible factor 1 (HIF-1) and HIF-2 in von Hippel-Lindau-associated renal cell carcinoma. *Mol Cell Biol* 2005, **25**(13)**:** 5675-5686.

117. Keith B, Johnson RS, Simon MC. HIF1alpha and HIF2alpha: sibling rivalry in hypoxic tumour growth and progression. *Nat Rev Cancer* 2012, **12**(1)**:** 9-22.

118. Hartley CJ, Reddy AK, Madala S, Michael LH, Entman ML, Taffet GE. Doppler estimation of reduced coronary flow reserve in mice with pressure overload cardiac hypertrophy. *Ultrasound Med Biol* 2008, **34**(6)**:** 892-901.

119. Li Q, Lin X, Yang X, Chang J. NFATc4 is negatively regulated in miR-133a-mediated cardiomyocyte hypertrophic repression. *Am J Physiol Heart Circ Physiol* 2010, **298**(5)**:** H1340-1347.

120. Chang J, Wei L, Otani T, Youker KA, Entman ML, Schwartz RJ. Inhibitory cardiac transcription factor, SRF-N, is generated by caspase 3 cleavage in human heart failure and attenuated by ventricular unloading. *Circulation* 2003, **108**(4)**:** 407-413.

121. Zhou Y, Li S, Huang Q, Xie L, Zhu X. Nanog suppresses cell migration by downregulating thymosin beta4 and Rnd3. *J Mol Cell Biol* 2013.

122. Boswell SA, Ongusaha PP, Nghiem P, Lee SW. The protective role of a small GTPase RhoE against UVB-induced DNA damage in keratinocytes. *The Journal of Biological Chemistry* 2007, **282**(7)**:** 4850-4858.

123. Poch E, Minambres R, Mocholi E, Ivorra C, Perez-Arago A, Guerri C, *et al.* RhoE interferes with Rb inactivation and regulates the proliferation and survival of the U87 human glioblastoma cell line. *Experimental Cell Research* 2007, **313**(4)**:** 719-731.

124. Bektic J, Pfeil K, Berger AP, Ramoner R, Pelzer A, Schafer G, *et al.* Small G-protein RhoE is underexpressed in prostate cancer and induces cell cycle arrest and apoptosis. *The Prostate* 2005, **64**(4)**:** 332-340.

125. Watanabe H. Rho-kinase activation in patients with pulmonary arterial hypertension. *Circulation Journal : Official Journal of the Japanese Circulation Society* 2009, **73**(9)**:** 1597-1598.

126. Do e Z, Fukumoto Y, Takaki A, Tawara S, Ohashi J, Nakano M, *et al.* Evidence for Rho-kinase activation in patients with pulmonary arterial hypertension. *Circulation Journal : Official Journal of the Japanese Circulation Society* 2009, **73**(9)**:** 1731-1739.

127. Zhang YM, Bo J, Taffet GE, Chang J, Shi J, Reddy AK, *et al.* Targeted deletion of ROCK1 protects the heart against pressure overload by inhibiting reactive fibrosis. *FASEB J* 2006, **20**(7)**:** 916-925.

128. Bao W, Hu E, Tao L, Boyce R, Mirabile R, Thudium DT, *et al.* Inhibition of Rho-kinase protects the heart against ischemia/reperfusion injury. *Cardiovasc Res* 2004, **61**(3)**:** 548-558.

129. Lai JM, Wu S, Huang DY, Chang ZF. Cytosolic retention of phosphorylated extracellular signal-regulated kinase and a Rho-associated kinase-mediated signal impair expression of p21(Cip1/Waf1) in phorbol 12-myristate-13- acetate-induced apoptotic cells. *Mol Cell Biol* 2002, **22**(21)**:** 7581-7592.

130. Petrache I, Crow MT, Neuss M, Garcia JG. Central involvement of Rho family GTPases in TNF-alpha-mediated bovine pulmonary endothelial cell apoptosis. *Biochem Biophys Res Commun* 2003, **306**(1)**:** 244-249.

131. Asano T, Ikegaki I, Satoh S, Suzuki Y, Shibuya M, Takayasu M, *et al.* Mechanism of action of a novel antivasospasm drug, HA1077. *J Pharmacol Exp Ther* 1987, **241**(3)**:** 1033-1040.

132. Ocaranza MP, Rivera P, Novoa U, Pinto M, Gonzalez L, Chiong M, *et al.* Rho kinase inhibition activates the homologous angiotensin-converting enzyme-angiotensin-(1-9) axis in experimental hypertension. *J Hypertens* 2011, **29**(4)**:** 706-715.

133. Matsumoto A, Manthey HD, Marsh SA, Fassett RG, de Haan JB, Rolfe BE, *et al.* Effects of exercise training and RhoA/ROCK inhibition on plaque in ApoE-/- mice. *Int J Cardiol* 2013, **167**(4)**:** 1282-1288.

134. Wu DJ, Xu JZ, Wu YJ, Jean-Charles L, Xiao B, Gao PJ, *et al.* Effects of fasudil on early atherosclerotic plaque formation and established lesion progression in apolipoprotein E-knockout mice. *Atherosclerosis* 2009, **207**(1)**:** 68-73.

135. Yasuda T, Tada Y, Tanabe N, Tatsumi K, West J. Rho-kinase inhibition alleviates pulmonary hypertension in transgenic mice expressing a dominant-negative type II bone morphogenetic protein receptor gene. *Am J Physiol Lung Cell Mol Physiol* 2011, **301**(5)**:** L667-674.

136. Schwenke DO, Pearson JT, Sonobe T, Ishibashi-Ueda H, Shimouchi A, Kangawa K, *et al.* Role of Rho-kinase signaling and endothelial dysfunction in modulating blood flow distribution in pulmonary hypertension. *J Appl Physiol (1985)* 2011, **110**(4)**:** 901-908.

137. Ziino AJ, Ivanovska J, Belcastro R, Kantores C, Xu EZ, Lau M, *et al.* Effects of rho-kinase inhibition on pulmonary hypertension, lung growth, and structure in neonatal rats chronically exposed to hypoxia. *Pediatr Res* 2010, **67**(2)**:** 177-182.

138. Ishiguro M, Kawasaki K, Suzuki Y, Ishizuka F, Mishiro K, Egashira Y, *et al.* A Rho kinase (ROCK) inhibitor, fasudil, prevents matrix metalloproteinase-9-

related hemorrhagic transformation in mice treated with tissue plasminogen activator. *Neuroscience* 2012, **220:** 302-312.

139. Zhang J, Bian HJ, Li XX, Liu XB, Sun JP, Li N, *et al.* ERK-MAPK signaling opposes rho-kinase to reduce cardiomyocyte apoptosis in heart ischemic preconditioning. *Mol Med* 2010, **16**(7-8)**:** 307-315.

140. Li Q, Xu Y, Li X, Guo Y, Liu G. Inhibition of Rho-kinase ameliorates myocardial remodeling and fibrosis in pressure overload and myocardial infarction: role of TGF-beta1-TAK1. *Toxicology letters* 2012, **211**(2)**:** 91-97.

141. Nohria A, Grunert ME, Rikitake Y, Noma K, Prsic A, Ganz P, *et al.* Rho kinase inhibition improves endothelial function in human subjects with coronary artery disease. *Circ Res* 2006, **99**(12)**:** 1426-1432.

142. Vicari RM, Chaitman B, Keefe D, Smith WB, Chrysant SG, Tonkon MJ, *et al.* Efficacy and safety of fasudil in patients with stable angina: a double-blind, placebo-controlled, phase 2 trial. *J Am Coll Cardiol* 2005, **46**(10)**:** 1803-1811.

143. Fukumoto Y, Mohri M, Inokuchi K, Ito A, Hirakawa Y, Masumoto A, *et al.* Anti-ischemic effects of fasudil, a specific Rho-kinase inhibitor, in patients with stable effort angina. *J Cardiovasc Pharmacol* 2007, **49**(3)**:** 117-121.

144. Shimokawa H, Hiramori K, Iinuma H, Hosoda S, Kishida H, Osada H, *et al.* Anti-anginal effect of fasudil, a Rho-kinase inhibitor, in patients with stable effort angina: a multicenter study. *J Cardiovasc Pharmacol* 2002, **40**(5)**:** 751-761.

145. Fujita H, Fukumoto Y, Saji K, Sugimura K, Demachi J, Nawata J, *et al.* Acute vasodilator effects of inhaled fasudil, a specific Rho-kinase inhibitor, in patients with pulmonary arterial hypertension. *Heart Vessels* 2010, **25**(2)**:** 144-149.

146. Kojonazarov B, Myrzaakhmatova A, Sooronbaev T, Ishizaki T, Aldashev A. Effects of fasudil in patients with high-altitude pulmonary hypertension. *Eur Respir J* 2012, **39**(2)**:** 496-498.

147. Li F, Xia W, Yuan S, Sun R. Acute inhibition of Rho-kinase attenuates pulmonary hypertension in patients with congenital heart disease. *Pediatr Cardiol* 2009, **30**(3)**:** 363-366.

148. Shibuya M, Hirai S, Seto M, Satoh S, Ohtomo E. Effects of fasudil in acute ischemic stroke: results of a prospective placebo-controlled double-blind trial. *J Neurol Sci* 2005, **238**(1-2)**:** 31-39.

149. Bain J, Plater L, Elliott M, Shpiro N, Hastie CJ, McLauchlan H, *et al.* The selectivity of protein kinase inhibitors: a further update. *Biochem J* 2007, **408**(3)**:** 297-315.

150. Parodi O, De Maria R, Oltrona L, Testa R, Sambuceti G, Roghi A, *et al.* Myocardial blood flow distribution in patients with ischemic heart disease or dilated cardiomyopathy undergoing heart transplantation. *Circulation* 1993, **88**(2)**:** 509-522.

151. Inoue T, Sakai Y, Morooka S, Hayashi T, Takayanagi K, Yamanaka T, *et al.* Coronary flow reserve in patients with dilated cardiomyopathy. *Am Heart J* 1993, **125**(1)**:** 93-98.

152. Opherk D, Schwarz F, Mall G, Manthey J, Baller D, Kubler W. Coronary dilatory capacity in idiopathic dilated cardiomyopathy: analysis of 16 patients. *Am J Cardiol* 1983, **51**(10)**:** 1657-1662.

153. Tsagalou EP, Anastasiou-Nana M, Agapitos E, Gika A, Drakos SG, Terrovitis JV, *et al.* Depressed coronary flow reserve is associated with decreased myocardial capillary density in patients with heart failure due to idiopathic dilated cardiomyopathy. *J Am Coll Cardiol* 2008, **52**(17)**:** 1391-1398.

154. Lee SH, Wolf PL, Escudero R, Deutsch R, Jamieson SW, Thistlethwaite PA. Early expression of angiogenesis factors in acute myocardial ischemia and infarction. *N Engl J Med* 2000, **342**(9)**:** 626-633.

155. Sano M, Minamino T, Toko H, Miyauchi H, Orimo M, Qin Y, *et al.* p53-induced inhibition of Hif-1 causes cardiac dysfunction during pressure overload. *Nature* 2007, **446**(7134)**:** 444-448.

156. Huang Y, Hickey RP, Yeh JL, Liu D, Dadak A, Young LH, *et al.* Cardiac myocyte-specific HIF-1alpha deletion alters vascularization, energy availability, calcium flux, and contractility in the normoxic heart. *FASEB J* 2004, **18**(10)**:** 1138-1140.

157. Xi L, Taher M, Yin C, Salloum F, Kukreja RC. Cobalt chloride induces delayed cardiac preconditioning in mice through selective activation of HIF-1alpha and AP-1 and iNOS signaling. *Am J Physiol Heart Circ Physiol* 2004, **287**(6)**:** H2369-2375.

158. Zhou J, Li K, Gu Y, Feng B, Ren G, Zhang L, *et al.* Transcriptional up-regulation of RhoE by hypoxia-inducible factor (HIF)-1 promotes epithelial to mesenchymal transition of gastric cancer cells during hypoxia. *Biochem Biophys Res Commun* 2011, **415**(2)**:** 348-354.